Dislocation dynamics and phase field crystal
A brief overview

Aymane Graini, Manas V. Upadhyay

*Laboratoire de Mécanique des Solides (LMS), École Polytechnique
07 November 2024

Contents

1 Introduction and aim **2**
1.1 Introduction . . . 2
1.2 Motivation and aim . . . 3

2 Modelling dislocations : An overview **4**
2.1 Introduction to dislocations . . . 4
2.2 Ab-initio modelling . . . 5
2.3 Molecular dynamics simulations . . . 6
2.4 Phase field crystal . . . 6
2.5 Discrete dislocations dynamics . . . 6
2.6 Continuous distribution of dislocations . . . 7
2.7 Continuum dislocation dynamics . . . 8
2.8 Field dislocation mechanics . . . 9
2.9 Field dislocation mechanics and phase field crystal . . . 11

3 Modelling tools summary **11**

4 Pattern formation and Swift-Hohenberg model **12**
4.1 Special case : 1-d SH model . . . 12
4.2 Amplitude equation . . . 13
4.3 The variational formulation of Swift-Hohenberg equation . . . 14
4.4 The concept of order parameter . . . 14
4.5 Topological defects in SH and PFC models . . . 15

5 Phase Field crystal model **17**
5.1 Introduction . . . 17
5.2 Time scale in PFC . . . 18
5.3 Dislocation dynamics with the PFC model . . . 19

6 Field dislocation mechanics and phase field crystal **21**

7 Kinematics of Burgers vector conservation **23**
7.1 Dislocation transport equation . . . 23
7.2 Kosevich's construction . . . 24
7.3 Evolution law of dislocation density tensor : . . . 25
7.3.1 Small deformations : . . . 25
7.3.2 Finite deformations : . . . 25
7.3.3 Additive decomposition of velocity gradient tensor: . . . 27

8 Constitutive analysis **28**
8.1 Mass balance 28
8.2 Momentum balance 28
8.3 Energy Balance 28
8.4 Entropy imbalance 28

Bibliography **30**

1 Introduction and aim

1.1 Introduction

Modeling plasticity in materials remains today a challenging task due to the interplay of different mechanisms occuring across multiple length scales, which are difficult to integrate into a single computational framework. Plastic deformation in crystalline solids, which manifests macroscopically as permanent deformations, originates from microscopic mechanisms heavily related to dislocations' nucleation, motion, and interactions. Ideally, a perfect crystal plasticty model would encompass relevant mechanisms at each length scale to determine macroscopic mechanical behavior; however, this is computationally unfeasible.

Classical plasticity theories in continuum mechanics address material yielding by introducing variables, such as plastic strain and some flow rules, to characterize the onset and evolution of plasticity. While effective for large-scale applications, these models are largely phenomenological; they rely on constitutive laws and parameters that must be empirically tuned or fitted to experimental data. In their heart, crystal plasticty approaches reflect an averaged, macroscopic behavior of dislocation ensembles, inevitably losing subscale information on the underlying microscopic processes. Consequently, classical models often struggle to accurately capture mesoscale effects. In contrast, microscopic theories like *Density Functional Theory* (**DFT**) (Woodward et al., 2008) and *Molecular Dynamics* (**MD**) (S. J. Zhou et al., 1998) provide detailed descriptions at atomic scales, capturing correct behaviors on short length and time scales. However, these methods are computationally prohibitive at larger time scales and mesoscopic length scales, making them impractical for predicting elasto-plastic responses and microstructural evolution over real-life timescales dimensions.
This gap between different models and scales has driven the development of mesoscale theories, aimed at bridging the microscopic and macroscopic scales in crystalline plasticity. Statistical physics introduced various coarse-graining approaches and helped formulating several mesoscale models. Among these, *Discrete Dislocation Dynamics* (**DDD**), a model that treats dislocations as discrete lines governed by the classical *Peach-Koehler* force, using stress fields derived from continuum mechanics (Devincre et al., 1992). DDD enables the investigation of mechanical properties on mesoscopic time and length scales while explicitly tracking dislocations. However, DDD models still rely on phenomenological prescriptions for dislocation mobility and interaction rules, which can limit their predictive accuracy.
To overcome the phenomenological nature of the previous models, *Field Dislocation Mechanics* (**FDM**) was introduced as a mesoscopic model in which dislocation lines are "smeared out" and represented by a continuous density field (Acharya, 2001) . This approach builds on earlier theories of continuously distributed dislocations, and the the dynamical theory of moving dislocations. FDM is a partial differential equation (PDE)-based theory in which atomic vibration kinetic energy is averaged out and exchanged for a dissipative evolution of dislocation density fields, encoded within the mathematical structure of the governing PDEs (Acharya, 2010). Furthermore, This PDE framework allows FDM to bypass the need for ad hoc rules for dislocations behavior and interactions. The FDM theory has a robust foundation, as it naturally reproduces several fundamental physical features of plasticity and dislocation mechanics (Zhang et al., 2015). However, its primary limitation lies in the absence of crystallographic

information within the free energy therein used. Without any crystalline information, the system's free energy remains convex, meaning that no restoring stresses act on dislocations to keep their cores compact, and no particular strain direction is energetically favored.

Within the realm of mesoscale and coarse-grained modeling, a widely used technique is the *Phase-Field* (**PF**) models as offers a robust framework for scale bridging. These models describe distinct phases using continuous order parameters, allowing for an implicit representation of interfaces between them. In particular, the *Phase Field Crystal* (**PFC**) model provides a mesoscale approach to capture the nonequilibrium dynamics of defected crystalline materials while accouting for elasticity (Elder et al., 2002), (Elder & Grant, 2004). It introduces a scalar field ψ, representing atomic density, alongside a free energy functional tailored to be minimized with the desired lattice symmetry. The evolution of this field is governed by dissipative conserved dynamics. In PFC, atomic vibrations where averaged out making the model valid only at diffusive timescales, similarily to FDM. However, PFC has the advantage of naturally incorporating topological defects and their evolution, the later being a common occurence in symmetry breaking phase transitions (Angheluta et al., 2012), and can be easily identfied within the amplitude expansion limit. As such, it has been widely used to study dislocations in crystals (Skogvoll, Angheluta, et al., 2022). Importantly, and due to its diffusive timescale, the PFC model struggles to capture elasticity and other wave-like behaviors accurately. The main issue being that the model rlies on a single scalar field to describe both atomic density and lattice distortion and it links the evolution of these variables to the slower, diffusive dynamics of the scalar field, which results in an unphyiscal behavior (Acharya et al., 2022). To address these limitations, various enhancements have been proposed in the literature. These include adding a second time derivative to the evolution equation (Stefanovic et al., 2006), introducing a dissipative current, displacing the scalar field with a compatible distortion to enforce equilibrium (Skaugen et al., 2018b), and even developing a full PFC-hydrodynamics theory (Skogvoll, Salvalaglio, & Angheluta, 2022). Nonetheless, these attempts often incorporate elasticity as a second step, or even like an afterthought.

In this work, we explore a novel approach to address the limitations of both PFC and FDM. We mentioned that, the PFC model accurately captures topological defects and their motion but lacks the ability to model elasticity, while FDM successfully models elasticity and dislocation mechanics but lacks crystallographic information. Thus, it seemed only natural to attempt a synthesis of the two theories to develop an ad hoc, physically accurate mesoscale model for dislocations. This approach, proposed in (Acharya & Viñals, 2020), is inspired by the *Peierls-Nabarro* model: we add a non-convex term in the free energy of the system, using the *Swift-Hohenberg* functional used in PFC modeling. A coupled FDM-PFC theory is then formulated and in which the scalar field ψ does not contribute to the elastic energy and is not interpreted as a mass density. Instead, the phase field serves solely as an indicator of defects, with its topological properties coupled to the elasticity of medium. By explicitly separating mass' motion and defect's motion, we investigate wether the new model will yield a correct framework to study dislocations' motion and plastity in crystalline material.

1.2 Motivation and aim

Update from presentation

2 Modelling dislocations : An overview

2.1 Introduction to dislocations

Crystals are a class of solid materials characterized by an ordered structure. Atoms occupy well defined sites in a pattern that repeats itself known as the *crystal structure*. In fact, the arrangement of atoms in a crystal can be described by a three-dimensional network of parallel lines, forming equal-sized parallelepipeds. The points where these lines intersect define a *Bravais* lattice, where each point has identical surroundings. A unit cell is the basic parallelepiped, and a crystal is formed by stacking identical unit cells in perfect alignment. By placing a group of atoms (motif) at each lattice point, the regular structure of a perfect crystal is created. This description only holds true for perfect crystal; however, in reality, crystals never are, and they suffer from several defects such as point-like, line, surface and even volume or bulk defects which renders them imperfect.
Throughout this whole work will focus on dislocations. Dislocations are line-like type of defects in crystals, perhaps first suggested in 1883 by Mügge (Mügge, 1883), who revealed and studied slip band within plastically deformed metals before their crystalline structure was discoverd, and couldn't understand the phenomena. Additionally, Voltera (Voltera, 1907) in 1907, and long before any possible experimental observation, characterized line defects in a perfect cylinder into 6 types: 3 translational (b,c and d) and 3 rotational (e,f and g) as illustrated in fig. 1. The translational line-like defect were later on named *dislocations*, however they were not linked to crystal plasticity until the last 1930s.

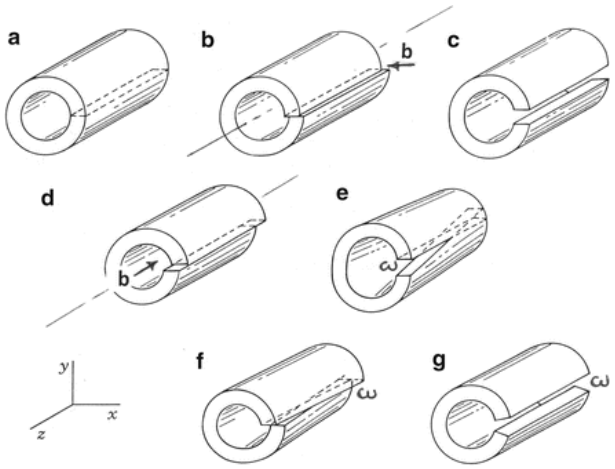

Figure 1: Line defects listed by Voltera (Voltera, 1907): (a) perfect cylinder, (b, c, d) are translational defects (dislocations) and (e, f, g) are rotational defects (disclinations).

Following the discovery of X-rays and X-ray diffraction, the crystalline structure of metals was established. After that, strong evidences for the presence of dislocations emerged from efforts to reconcile theoretical and experimental values of the shear stress required for plastic deformation of a single perfect crystal. This can be traced back to *Frenkel*'s work in 1926 (Frenkel, 1926). In an ideal crystal, the slip of one atomic plane over an adjacent plane would require a coordinated, rigid motion of all atoms from one position of perfect alignment to another. *Frenkel* (Frenkel, 1926) proposed that the shear force needed to slide the upper row of atoms over the lower row follows a periodic, sinusoidal function.

$$\tau = \frac{Gb}{2\pi a} \sin \frac{2\pi x}{b} \quad \Rightarrow \quad \tau_{max} = \frac{b}{a} \frac{G}{2\pi} \tag{1}$$

This assumption revealed that the theoretical estimate of shear stress limit of a perfect crystal is several order of magnitude of those experimentally observed. This significant discrepancy between theory and experiment was explained in 1934 by the simultaneous and independent

works of Orowan (Orowan, n.d.), Polanyi (Polanyi, n.d.), and Taylor (Taylor, 1934) through the consideration of dislocations motion and its role in the mechanism behind plastic deformation of crystals. This also gave birth to the well-known model of caterpillar or carpet as an illustration to plastic deformation induced by dislocations motion in crystals, see fig. 2.

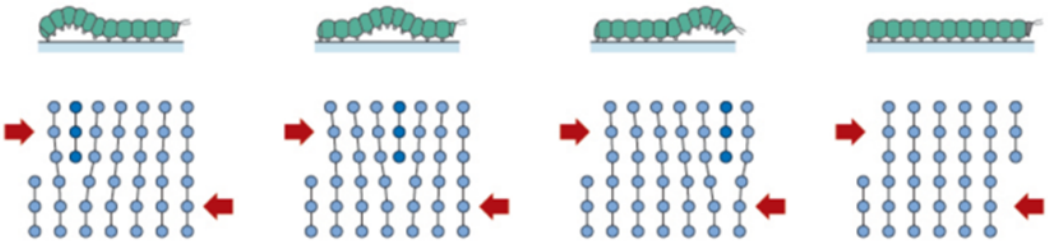

Figure 2: Line defects listed by Voltera (Voltera, 1907): (a) perfect cylinder, (b, c, d) are dislocations and (e, f, g) are disclinations.

The existence of dislocations is also implied by studies of crystal growth. Studies of nucleation by Volmer (1939) followed the ideas of Gibbs (1948) and suggested that nucleation of new layers during growth of perfect crystals required supersaturations of about 1.5. However, experiments showed that crystals grew under nearly equilibrium conditions. The difficulty was resolved by Frank in 1949XX, by postulating that growth could proceed at lower supersaturations, by the propagation of ledges that are present where spiral dislocations intersect surfaces.
Since then, the presence and effects of dislocations have been recognized as significant. As a result, dislocations have been extensively studied to understand and quantify their impact on the properties of various material classes, including metals and semiconductors. Over the past fifty years, scientific advances have led to the development of methods for observing and modeling dislocations at different scales. Given the focus of this thesis on dislocation modeling, we will start by briefly reviewing the tools and models available in the literature for this purpose.

2.2 Ab-initio modelling

At the atomic level, quantum mechanics based models offer the most fundamental and accurate description of the underlying physics of dislocations. They're often deemed first principle calculations or Ab Initio simulations. These models rely on the so called *Born-Oppenheimer* approximation: Atomic nuclei due to their mass, are assumed to be fixed and the problem is simplified into only solving for the evolution of the electrons by means *Shrödinger*'s equation. *Density Functional Theory* (DFT) is the most commonly used method for numerically solving *Shrödinger*'s equation. Inferring to *Hohenberg-Kohn* theorems (Engel & Dreizler, 2011) which allows one to bypass the need to solve for each electron individually, in DFT electrons' spatial distribution is replaced by as scalar function called electronic density which obeys Kohn-Sham equations.
There are available libraries such as, *QuantumEspresso* or *VASP* which allows optimized numerical solution to *Kohn-Sham* equations. But DFT simulations remain computationally intensive, and scale cubically with the number of atoms, so that their often limited to few hundred of atoms. As a consequence, DFT calculations generally focus on dislocation core's structure (Woodward et al., 2008) and energy and give insight onto fundamental and local properties of dislocations such as cross slip, nucleation, selection of glide planes and mobility of dislocations (Rodney et al., 2017). Recently, these models explored quantum effects of atomic nuclei on lattice resistance in BCC materials (Proville et al., 2012), allowing better estimates and better understanding of *Peierls stress* needed to move a dislocation within a plane of atoms.

In addition, these ab initio models have been widely used to generate material property databases for developing interatomic potentials (Payne et al., 1996): a key ingredient for classical molec-

ular dynamics models that operate at the next scale as presented in the following section.

2.3 Molecular dynamics simulations

At a molecular level, i.e on the scale of few hundreds of nm, *molecular dynamics* (MD) and *molecular statics* (MS) are used. Considered systems consists of classically described atoms interacting with each other with a given interaction potential U. The main variables are just atomic positions $\{\boldsymbol{r_i}\}$ and their time evolution is prescribed by Newton's equation of motion:

$$m_i \frac{d^2 \boldsymbol{r_i}}{dt^2} = -\boldsymbol{\nabla} U(\boldsymbol{r}) \quad \forall\, i \tag{2}$$

Molecular dynamics have been widely used to study dislocations properties such as line energies (X. W. Zhou et al., 2017), mobilities (Olmsted et al., 2004), cross-slip rates (Rao et al., 2011), interactions between dislocations (S. J. Zhou et al., 1998), and with other defects (Spearot & Sangid, 2014).
Optimized algorithm for the numerical integration of the equation of motion are commonly available today, such as *LAMMPS* (Thompson et al., 2022). However, the major challenge in molecular simulations is post-processing: Analyzing atomic trajectories in order to identify dislocations from atomic positions. Algorithms, such as the *Dislocation Extraction Algorithm* (DXA) (Stukowski & Albe, 2010), automatically and efficiently detects dislocations and extracts their corresponding Burgers vector.

Although being less computationally expensive than ab initio methods, MD simulations of metals are still limited to systems of $\sim 10^6$ atoms. Moreover, integration of the equations of motion requires very small time steps ($\sim 1\ fs$), so that the total duration of a simulation is around $10ns$ if we perform 10^7 timestep which limits the application of MD simulations to very high strain rate scenarios, usually $> 10^6\ s^{-1}$.

2.4 Phase field crystal

2.5 Discrete dislocations dynamics

At somewhat larger scale ($\sim \mu m$), a popular technique known as *Discrete Dislocation dynamics* (DDD) (Devincre et al., 1992) (Kubin & Canova, 1992) is often used. It aims at retaining the discrete nature of dislocations in crystals while providing enough computational capabilities to exceed the time and space scale limitations of molecular simulations. The idea is to couple the motion of the discrete dislocations with a continuum elastic description of the medium in which they're embedded (Bulatov & Cai, 2006).

Each dislocation line, let's say of index i, is discretized into $\{\boldsymbol{r_j}\}_{1\leq j\leq N}$ node each with its own Burgers vector $\boldsymbol{b_{ij}}$. At each time step, the stress field $\boldsymbol{\sigma}$ is computed using linear elasticity which induces a Peach-Köehler force $\boldsymbol{F_i}$ on each dislocation line to which some additional forces might be added if considered such as (Peierls, interaction, obstacle, osmotic, thermal, ...). Using a mobility Law $\boldsymbol{V_i} = M(\boldsymbol{F_i^{tot}})$, the position of each dislocation is updated by a time integration of :

$$\frac{d\boldsymbol{r_i}}{dt} = g_i(\{\boldsymbol{r_j}\}, \dots) \tag{3}$$

After updating the position of each dislocation line, a special algorithm is needed to keep track of all dislocations and detects' possible collisions. Following this step, a set of well-defined and prescribed rules is used to handle interactions and topological changes such as junction formations, intersections, annihilation, cross slip, nucleation etc... Optimized open-source codes are available to perform DDD simulations like ParaDiS (T. Arsenlis, V. Bulatov, W. Cai, G. Hommes, M. Rhee, and M. Tang., 2021) developed at Stanford University, and TriDis ("TriDis", 2021) developed at SIMaP in Grenoble. Even though *GPU* acceleration has been proposed

(Bertin et al., 2019) which allowed large scale DDD simulations within reasonable running time, computational cost is still too high if one aims at replicating the strain rates typically used in experimental setups. Recently, an attempt has been proposed by coupling DDD to Finite elements (Cui et al., 2021), in order to study Dislocation evolution during thermo-mechanical loading of tungsten.

2.6 Continuous distribution of dislocations

Before attempting to move to a larger scale, it is important to have an estimate of the amount of dislocations stored in crystal. For this aim, we introduce a scalar quantity : the dislocation density ρ^d which is the defined as the total length of all dislocation lines per unit volume. In an undeformed metal, the dislocation density is often $\sim 10^8\, m^{-2}$, However heavily deformed metals exhibits high dislocation densities $\sim 10^{15}\, m^{-2}$ (Kochmann, 2009). Due to this high density, it would be inefficient and quite impossible to handle the excessive amount of dislocations when working in scale of $\sim cm$, for which the total length of dislocation lines would be around $1000\, km$. For this purpose, the static continuum theory of dislocations was introduced by *Nye* (Nye, 1953), *Bilby* (Bilby et al., 1955), *Kröner*(Kröner, 1959) and *Willis* (Willis, 1967a), and further formalized using modern statistical mechanics and thermodynamics by *Berdichvsky* (Berdichevsky, 2006).

The continuum theory of dislocations treats the behavior of the large ensemble of dislocations in the medium by means of common continuum mechanics, using an explicit dependence of the free energy of the system on the dislocations density. The tenet of the theory is the so called dislocation density tensor $\boldsymbol{\alpha}$ introduced by *Nye* (Nye, 1953) to take into account the *geometrically necessarily dislocations* (GNDs). Nye used geometrical arguments to link the curvature tensor $\boldsymbol{\kappa}$ to the dislocation density tensor $\boldsymbol{\alpha}$:

$$\boldsymbol{\kappa} = \boldsymbol{\alpha} - \frac{1}{2}\mathbf{Tr}\,\boldsymbol{\alpha}\,\mathbb{I} \tag{4}$$

Kröner (Kröner, 1959) formalized the definition of the dislocation density tensor $\boldsymbol{\alpha}$ as the fundamental measure of incompatibility, and established its link with and the plastic distortion $\boldsymbol{U}^p$ in a small deformation setting.
Given a surface $\mathcal{S}$ inside the medium bounded by a closed circuit $\mathcal{C}$, he noted that :

$$\iint_{\mathcal{S}} \boldsymbol{\alpha}\cdot\boldsymbol{da} = \iint_{\mathcal{S}} \mathbf{curl}\,\boldsymbol{U}^p\cdot\boldsymbol{da} = \oint_{\mathcal{C}} \boldsymbol{U}^p\cdot\boldsymbol{dl} = \boldsymbol{b_c} \quad \text{with} \quad \boldsymbol{\alpha} := \mathbf{curl}\,\boldsymbol{U}^p \tag{5}$$

Following this definition, the dislocation density tensor $\boldsymbol{\alpha}$ is a second order tensor that gives for any arbitrary closed circuit $\mathcal{C}$ the resulting Burgers vector $\boldsymbol{b_c}$ of all dislocation lines threading through it. Which suggests to interpret $\boldsymbol{\alpha}$ as line density where each line carries some Burgers vector, so that locally, at least, we can write $\boldsymbol{\alpha} = \boldsymbol{b_c}\otimes\boldsymbol{t}$ where $\boldsymbol{t}$ is the tangent vector to a dislocation line, or the normal vector to an infinitesimal surface $\boldsymbol{da}$.
After introducing $\boldsymbol{\alpha}$, the first problem addressed was on how to find the stress field produced by a given dislocation density $\boldsymbol{\alpha}$. It was elegantly solved by *Kröner* (Kröner, 1959) in 1598 in a linear setting. Then, the same problem was solved by Willis (Willis, 1967b) but in a finite deformation framework while also accounting for material anisotropy.

The so far presented works only apply for the static case. It was only due to the work of *Mura* (Mura, 1963) in 1963, *Fox* (Fox, 1966) in 1966 and *Kosevich* (Kosevich, 1965) in 1979, that a full dynamical theory of moving dislocations was established. The authors, from different derivations, obtained the following evolution equation of the dislocation density tensor:

$$\dot{\boldsymbol{\alpha}} = -\mathbf{curl}\left(\boldsymbol{\alpha}\times\boldsymbol{v}^d\right) \tag{6}$$

Where $\boldsymbol{v}^{\boldsymbol{d}}$ is the dislocation velocity vector. The term $\boldsymbol{\alpha} \times \boldsymbol{v}^{\boldsymbol{d}}$ was interpreted as *dislocation flux density* by *Kosevich* (Kosevich, 1965), and was understood as the plastic strain rate induced by dislocation motion. The physical interpretation was further analyzed by *Acharya* in (Acharya, 2011).

It was quickly understood that the continuum theory of dislocations raises a fundamental issue when treating the dislocation core : Stresses diverges within the core, the incompatible elastic displacement is discontinuous and more importantly the core cannot be kept compact and localized. The issue was first addressed by *Peierls* in 1940 (Peierls, 1940), in the case of a single edge dislocation. If the core is represented as a continuous distribution, the stress around it tend to spread it out independent and equilibrium structure of the core can be maintained. This can be understood using the fact that two dislocations of the same sign tend to repel each other so that a continuous description of the core of a single dislocation will naturally diffuse until it uniformly vanishes. Peierls (Peierls, 1940) argued that a stable compact core is maintained if the internal stress from the continuous distribution is balanced by a restoring force that reflects the underlying crystal structure. His model was later extended by *Nabarro* (Nabarro, 1947) in 1947, which became the well known *Peierls-Nabarro* model. The model introduced a sinusoidal restoring stress T^R that depends on the misfit η, originally introduced for an edge dislocation in a infinite simple cubic crystal :

$$T^R = \frac{\mu}{2\pi} \sin\left(2\pi \frac{\eta}{b}\right) \quad \text{with} \quad \eta(x) = \frac{b}{2} + \frac{b}{\pi} \arctan\left(2(1 - \nu \frac{x}{b})\right) \tag{7}$$

In addition, this resorting stress can be used to construct a regularization of total elastic energy in order to treat the discontinuity of the incompatible elastic displacement within the core of the dislocation. The new term adds a non-convex part to the total energy (Fressengeas, 2017), from which an equilibrium compact core can be found. It reads:

$$\Psi = \psi(\epsilon^e) + \frac{\gamma}{d} \quad \text{with} \quad \gamma = \frac{\mu b}{4\pi^2}\left(1 - \cos\left(2\pi \frac{\eta}{b}\right)\right) \tag{8}$$

Furthermore, one of the major shortcomings of the theory of continuously distributed dislocations is the resolution size dependence on the Burgers circuit $\mathcal{C}$ used to detect dislocations, the main issue being that only the resulting Burgers vector is measured through $\boldsymbol{\alpha}$ (Kröner, 2001). This means that all the positive and negative dislocations cancel each other to a very large amount. The Kroner-Nye dislocation tensor only captures, if one works on a meso/macroscale, the so called geometrically necessary dislocations (GNDs) and overlooks all the statistically stored dislocations (SSDs) (Sandfeld et al., 2011). As a result, it overlooks the complex internal structure of the dislocation network, leading to an incomplete description of the internal mechanical state. As a consequences, all theories based on the *Kröner-Nye* tensor need to be patched up by phenomenological terms to take into account averaged out dislocations when modeling meso/macroscale plastic deformations. An example is the phenomenological mesoscale field dislocation mechanics suggested by *Acharya* and *Roy* (Acharya & Roy, 2006). The dislocation transport of the mesoscopic space-times averaged field variables $\overline{\boldsymbol{\alpha}}$ and $\overline{\boldsymbol{V}}^{\boldsymbol{d}}$ is given by (Acharya & Roy, 2006):

$$\overset{\circ}{\overline{\boldsymbol{\alpha}}} = -\mathbf{curl}\left(\overline{\boldsymbol{\alpha}} \times \overline{\boldsymbol{V}}^{d} + \boldsymbol{L}^{\boldsymbol{p}}\right) + \boldsymbol{s} \tag{9}$$

Where $\boldsymbol{L}^{\boldsymbol{p}}$ is the plastic strain rate produced by the statistical dislocations (microscopic) which is not accounted for in $\overline{\boldsymbol{\alpha}} \times \overline{\boldsymbol{V}}^{d}$, and $\boldsymbol{s}$ is a dislocation nucleation rate term. Both $\boldsymbol{L}^{\boldsymbol{p}}$ and $\boldsymbol{s}$, (as well as dislocation velocity) should be prescribed constitutively depending on the desired model. Examples of $J2$ plasticity and crystal plasticity are given in (Arora, 2019).

2.7 Continuum dislocation dynamics

It was already pointed out that the classical *Kröner-Nye* dislocation tensor averages overall several dislocation lines to yield their resultant Burgers vector (Kröner, 2001) , so that information

on the microscopic statistical dislocations is lost. In addition, it is important to understand that the kinematic information stored in $\boldsymbol{\alpha}$ is only reliable if all dislocation lines threading through the circuit are parallel: if they differ in orientation the resulting average is necessarily altered.

A different apporoach proposed by *Hochrainer* (Hochrainer et al., 2007) (Hochrainer et al., 2014), in his continuum dislocation dynamics theory. He introduces what he calls the *second order dislocation density tensor* (**SODT**) $\boldsymbol{\alpha}^{II}$ that lives on higher dimensional space ($\mathbb{R}\otimes\mathbb{R}\otimes\mathbb{S}^1$), in contrast to $\boldsymbol{\alpha}\in\mathbb{R}\otimes\mathbb{R}$. The SODT $\boldsymbol{\alpha}^{II}$ distinguishes dislocations a priori by their line direction before any averaging is introduced: it consider the angle φ between the tangential vector $\boldsymbol{t}$ and its Burgers' vector $\boldsymbol{b}$. Hence, it is able to describe the kinematics of very general systems of dislocations. It was shown that the SODT simplifies to the classical *Kröner-Nye* tensor. The former is uniquely defines by the scalar dislocation density ρ^d and the curvature density κ^d, which are also used to derive coupled evolution equations.

2.8 Field dislocation mechanics

Field dislocation mechanics (**FDM**) is a continuum theory for crystal plasticity proposed by *Acharya* in 2001 (Acharya, 2001) following the works of *Willis* (Willis, 1967b), *Kröner* (Kröner, 1959), *Fox* (Fox, 1966), *Mura* (Mura, 1963) and *Kosevich* (Kosevich, 1965). As explained in (Acharya, 2001), FDM is introduced as an attempt to extend and improve the *elastic theory of the continuously distributed dislocations* (**ECDD**) presented in (Willis, 1967b) for which the main issue is the lack of the two-way interaction between stress state and dislocation field. In addition, the problem as initially posed in ECDD is ill-posed : given an inverse elastic distortion $\boldsymbol{W}$, one can compute a unique dislocation field $\boldsymbol{\alpha}$; however, given $\boldsymbol{\alpha}$, uniqueness of $\boldsymbol{W}$ is lost because they're related by $\mathbf{curl}\,\boldsymbol{W}=-\boldsymbol{\alpha}$ and $\boldsymbol{W}+\boldsymbol{\nabla f}$ is a solution for any vector field $\boldsymbol{f}$. The idea behind *Acharya*'s work in an orthogonal decomposition using the null space of the $\mathbf{curl}$ operator of tensors into compatible and incompatible parts, which enables a unique determination of the deformation field by adding an additional equation governing $\boldsymbol{\nabla f}$ using constitutive analysis as performed by *Acharya* in (Acharya, 2004). The inverse elastic distortion is decomposed into compatible and incompatible parts (which will later on understood as a generalization of Stokes-Helmholtz decomposition to higher order tensors):

$$\begin{aligned}
&\boldsymbol{W}=\boldsymbol{\chi}+\boldsymbol{\nabla f}\quad\text{with}\quad\boldsymbol{W}={\boldsymbol{F_e}}^{-1}\\
&\mathbf{curl}\,\boldsymbol{W}=\mathbf{curl}\,\boldsymbol{\chi}=-\boldsymbol{\alpha}\\
&\mathbf{div}\,\boldsymbol{\chi}=0\\
&\mathbf{div}\,(\boldsymbol{\nabla}\dot{\boldsymbol{f}})=\mathbf{div}\,(\boldsymbol{\alpha}\times\boldsymbol{v^d}-\dot{\boldsymbol{\chi}}-\boldsymbol{\chi L})
\end{aligned}\tag{10}$$

The constitutive analysis also exposes the driving force acting on the dislocations as a non linear generalization of the classical *Peach-Koehler* forces (Acharya, 2003), (Acharya, 2004):

$$\boldsymbol{f^d}:=\rho\left(\frac{\partial\psi}{\partial\boldsymbol{W}}\right)^t\boldsymbol{\alpha}:\boldsymbol{\mathcal{E}}\tag{11}$$

In addition, the dislocation transport equation used is the same as the one derived by *Mura* (Mura, 1963) and (Kosevich, 1965), i.e $\dot{\boldsymbol{\alpha}}=-\mathbf{curl}\left(\boldsymbol{\alpha}\times\boldsymbol{v^d}\right)$. In (Acharya, 2003), *Acharya* derives the necessary boundary conditions on $\boldsymbol{\alpha}$ for the closure of the dislocation transport equation which reduces to the specification of the dislocation flux $\boldsymbol{v^d}\cdot\boldsymbol{n\alpha}=F_\alpha$ on the inflow boundary $\partial\Omega_t^-$ where $\boldsymbol{v^d}\cdot\boldsymbol{n}<0$. In its early stages and shortly after its foundation had been posed, FDM theory proved itself by successfully representing various physical features such as local Schmid and non-Schmid behaviors, yielding (Acharya, 2003), and the formation of a slip step when a moving dislocation meets a free surface boundary (Acharya, 2001). In addition, it was shown that the theory reduces to classical non linear elasticity when no dislocations are involved, and to classical theory of continuously distributed dislocations when no velocity is

considered (Acharya, 2004). One of the main advantages of FDM, is that dislocations are treated as a continuous field and their time evolution is PDE-dictated, bypassing any need to prescribe interaction rules (like those used in DDD) So that the increasing number of dislocations has no computational cost. As demonstrated in (Varadhan et al., 2006), the transport equation used in FDM is able to model expansion, annihilation and shocks of dislocations. Another conceptual advantage, is that FDM do not introducing neither an intermediate nor a reference configuration, so that the multiplicative decomposition of the distortion into plastic $\boldsymbol{F}_p$ and elastic $\boldsymbol{F}_e$ is not postulated (Acharya & Zhang, 2015). Instead, it is assumed that at each time step, the body can be, by thought, mapped to a relaxed stress free configuration which is fictitious and not necessarily connected. The relaxed configuration serves as a way to introduce the (inverse) elastic distortion and the Burgers vector (Fressengeas, 2017): A closed curve in the current configuration is not necessarily closed when pulled-back to the relaxed one, the failure in closure is the Burgers vector given in units of the undeformed lattice in the relaxed configuration. Even though no multiplicative decomposition is postulated in the theory, an additive decomposition of the velocity gradient naturally emerges from the conservation of Burgers vector (Acharya & Zhang, 2015).

Field dislocation mechanics is continuum theory in which kinetic energy of atomic vibrations (and all energy below a given length scale) have been averaged out exchanged with a dissipative evolution of continous density fields encoded in the mathematical structure of the PDEs governing the evolution (Acharya, 2010). The theory was introduced as an attempt to model crystal plasticity at a time scale of $\sim \mu s$ and more, however it was previously argued the averaged nature of the theory makes it unvalid at larger length scales since it doesn't account for the statistically stored disclocations and it is necessary to back it up with phenomenological assumptions. It is in this puropose that the phenomenological mesoscopic field dislocation mechanics was introduced in 2006 (Acharya & Roy, 2006). The newly introduced theory is merely a space-time average of the previously developed Field dislocation mechanics followed by closure assumptions, and by constitutive prescription of the plastic strain rate of the statistically stored dislocations. With that being said, FDM can be seen a bridge between elastolpasticity and dislocation theory which were always treated as separate topics, it also includes several physical aspecets of crystal plasticty. Nonetheless, There are still some fundamental issues to be adressed, namely on relevance of the core energy regulariziation (Acharya & Tartar, 2011), on the existence of a *Peierls* stress threshold to the onset of dislocation motion which was proved to exist in some special cases (Acharya, 2010) (Zhang et al., 2015), on the inclusion of crystalline structure in order to keep a compact core (Acharya, 2010), and the speed of propagation of elasatic waves in the dynamis of dislocations (Zhang et al., 2015). Additionally, the FDM theory as porposed and developed through the years remained isothermal until the *Thermal-FDM* was porposed by *Upadhyay* in (Upadhyay, 2020). *Thermal-FDM* (*T-FDM*) introduces a strong coupling between dislocation mechanics and heat conduction, targeting dislocation dynamics under rapid or gradual temperature changes, such as in heat-affected crystalline solids during additive manufacturing, to model temperature changes can drive dislocation behaviors, and vice versa.

The first numerical implementation of field dislocation mechanics (FDM) goes back to *Roy* and *Acharya* in 2005 (Roy, 2005), who developed a finite element solver for both static and moving dislocations within the small deformation limit, albeit with a constant velocity constraint (since stress coupling hindered maintaining a compact dislocation core). Then, the following studies focused on the dynamics of dislocation transport, such as the work by *Varadhan* (Varadhan et al., 2006), which explored a purely kinematic dislocation evolution, where velocity and stress fields were also uncoupled. Their simulations demonstrated that FDM accurately captured essential behaviors like shock formation, wave propagation, and annihilation events, as seen in the expansion of a polygonal loop and the operation of a *Frank-Read* source. It was until

2020, that *Arora* developed a finite element implementation of the mesoscopic field dislocation mechanics capable of handling large deformations (Arora et al., 2020). Their work first demonstrated non-linear elasticity in dislocation-free conditions, then it was used to analyze stress fields in cases involving isolated dislocations and homogenous dislocation densities. They numerically confirmed that a spatially homogenous dislocation density is not stress-free when geometric non-linearities are taken into account, corroborating previous theoretical predictions (Acharya, 2018). Furthermore, the model successfully reproduced the formation of slip steps and shear bands without ad-hoc failure criteria in the stress-uncoupled case, along with Mach cone formation for supersonic dislocation velocities. This implementation of mesoscopic FDM also demonstrated the emergence of complex dislocation patterns and realistic microstructural features of crystal plasticity (Arora & Acharya, 2020). To tackle the stress-coupled case, *Arora* introduced a non-convex term (see eq. (12)) inspired by the *Peierls-Nabarro* model (Nabarro, 1947), which depends a new state variable $\boldsymbol{P}$, enabling the annihilation of two edge dislocations while maintaining a compact core (Arora, 2019).

$$\psi(\boldsymbol{W},\boldsymbol{\alpha},\boldsymbol{P}) = \varphi_e(\boldsymbol{W}) + \Upsilon(\boldsymbol{\alpha}) + \underbrace{\eta(\boldsymbol{P})}_{\text{extra term}} \quad \text{with} \quad \eta(\boldsymbol{P}) = \frac{C}{\rho^*}\left[1-\cos\frac{2\pi P_{12}}{\omega}\right] \tag{12}$$

Most recently, a finite element implementation of the small deformation limit of thermal field dislocation mechanics (T-FDM) was achieved, expanding on previous isothermal models by integrating temperature effects. The model allows for explicit simulation of how dislocations impact temperature profiles and vice versa (Lima-Chaves & Upadhyay, 2024).

Despite its promising framework for simulating dislocation mechanics without ad-hoc interaction rules, *Field Dislocation Mechanics* (**FDM**), has some essential limitations. Previously, we identified a major limitation: FDM does not inherently account for the underlying crystalline structure of the material. This limitation affects the ability of dislocation cores to remain compact and hinders the coupling between stress and dislocation velocity. To address this, a coupling between FDM and the *Phase Field Crystal* (**PFC**) model was proposed (Acharya & Viñals, 2020). The PFC model, a phase-field approach within the domain of complex pattern formation, employs a *Swift-Hohenberg* type of energy functional, which is minimized to generate a desired crystalline structures. Integrating PFC with FDM introduces a non-convex energy term that enhances the representation of crystal structures within the formulation of FDM. Prior to diving into the specifics of the PFC-FDM coupling, we first provide in the upcoming section an overview of pattern formation theories and the PFC model.

2.9 Field dislocation mechanics and phase field crystal

3 Modelling tools summary

Technique	Length scale	Time scale	Crystal.	Evolution	Elasticity
Q-DFT	$\mathring{A}$	fs	Natural	Kohn-Sham	Yes
MD	nm	$\sim ps, \sim ns$	Natural	Newton	Yes
PFC	nm	Diffusive	Natural	Disspative Flow	No
DDD	μm	ns	Prescribed	Kinetic laws	Yes
FDM	Mesoscale	Diffusive/Quasi-static	Prescribed	Conservation laws	Yes
CP	$\sim \mu m, \sim mm$	Quasi-static	Prescribed	Constitutive+Rules	Yes

4 Pattern formation and Swift-Hohenberg model

The first quantitative experiments and studies of pattern formation due to convection can be traced back to *Henri Bérnard* (Bénard, 1901). He studied the stability of a thin fluid layer open to air and submitted to a vertical temperature gradient. He accurately determined periodicity of the hexagonal pattern, as illustrated in fig. 3. After that, Lord Rayleigh (Rayleigh, 1916) proposed a theory based on a feedback coupling due to buoyancy in which a hot fluid particle hotter than its environment encounters ever colder fluid as it rises, which leads to the instability, and lead to the generation of convective currents. This instability later known as *Rayleigh-Bérnard* instability was a a subject of several studies, namely the inclusion of surface tension effect.

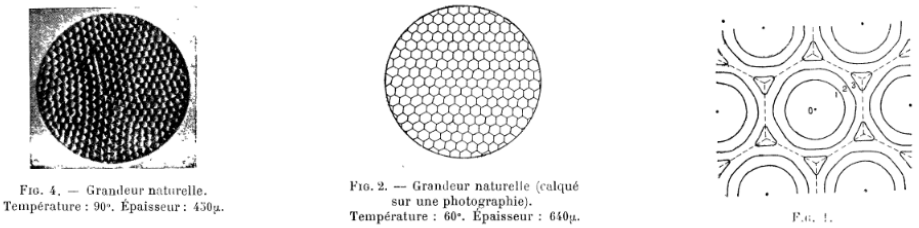

Figure 3: Convection cells in *Rayleigh-Bérnard* instability, from (Bénard, 1901)

One of its main features is that *Rayleigh-Bérnard* convection exhibits well-ordered structure but that are formed under non-equilibrium conditions, (in contrast to crystalline materials). Fundamental questions concern the processes underlying the determination of the wavelength, and about the onset of the instability and how it is related to thermal fluctuations. *Swift* and *Hohenberg*, in 1977, proposed a model based on hydrodynamic fluctuations in order to study to what extent the non-equilibrium transition from a uniform to non uniform convecting state was similar to an equilibrium phase transition (Swift & Hohenberg, 1977). Their model was also aimed at understanding the effect of thermal fluctuations on this convective instability. They introduce order parameter $\psi(\boldsymbol{x}, t)$ which is meant to represent the vertical velocity of temperature fluctuation at the mid plane of the convective cell. The *Swift-Hohenberg* model gives the evolution equation of ψ as:

$$\tau_0 \frac{\partial \psi}{\partial t} = \left[\epsilon - \frac{\xi_0^2}{4q_c^2}\left(\nabla^2 + q_c^2\right)^2\right]\psi - g(\mathrm{Pr})q_c^2\psi^3 \tag{13}$$

Where, we mainly highlight the fact that ϵ is the deviation of *Rayleigh* number from its critical value. The previous equation can be rescaled to the following, classical form:

$$\frac{\partial \psi}{\partial t} = \left[\epsilon - \left(\nabla^2 + q_0^2\right)^2\right]\psi - \psi^3 \tag{14}$$

4.1 Special case : 1-d SH model

One can gain much physical insight on the previous equation if we limit ourselves to the 1 dimensional case:

$$\frac{\partial \psi}{\partial t} = \left[\epsilon - \left(\partial_x^2 + q_0^2\right)^2\right]\psi - \psi^3 \tag{15}$$

It it obvious that the homogeneous field $\psi_h = 0$ is a solution of the 1-D *Swift-Hohenberg* equation. In order to investigate wether this homogeneous solution, is stable as we vary the parameter ϵ. We would like to determine the critical value ϵ_c when the state $\psi_h = 0$ becomes linearly unstable, i.e. when the magnitude of an arbitrary infinitesimal perturbation $\delta\psi$ begins to grow exponentially in time.

Let's consider a perturbed field $\psi = \psi_h + \delta\psi$. At the first order in $\delta\psi$, neglecting higher powers, we find that it satisfies:

$$\partial_t \delta\psi = \left(\epsilon - q_0^4 - \partial_x^4 - 2q_0^2\partial_x^2\right)\delta\psi \tag{16}$$

This linear differential equations admits a particular solution in the form of :

$$\delta\psi(x,t) = Ae^{\sigma t}e^{\alpha x} \tag{17}$$

Replacing in the previous equation, one finds that:

$$\sigma = \epsilon - (\alpha^2 + q_0^2)^2 \tag{18}$$

If the domain is spatial infinite then x can go to $\pm\infty$, in that case, we necessarily must have $\alpha \in i\mathbb{R}$ is a purely imaginary number, because if not then $\delta\psi$ is not a small perturbation (at least at $t = 0$).
If the domain is periodic over length L, then one must have $\alpha L = (2\pi m)$ for $m \in \mathbb{Z}$. So that, in any case, we write $\alpha = iq \in i\mathbb{R}$, with $q \in \mathbb{R}$. Finally, we get:

$$\sigma(q) = \epsilon - (-q^2 + q_0^2)^2 \tag{19}$$

Due to the linear nature of the differential equation eq. (16), a general solution can be written as :

$$\delta\psi(x,t) = \int_{-\infty}^{+\infty} A_q e^{\sigma(q)t}e^{iqx}\,dq \tag{20}$$

If $\epsilon < 0$, then $\sigma(q) < 0\,\forall\, q$, meaning that all perturbations $\delta\psi$ decay exponentially in time $t \to \infty$. This translates to the fact that the homogeneous state $\psi_h = 0$ is linearly stable. However, as soon, as $\epsilon = \epsilon_c = 0$, stability is lost for the mode $q = \pm q_0$, and as soon as $\epsilon > 0$, ever slightly, the domain where $\sigma(q) > 0$ gets bigger and Fourier modes with vector close to q_0 will exponentially grow in time. This suggest, the onset of pattern formation and predicts the formation of some cellular structure with a characteristic wavelength $2\pi/q_0$.

4.2 Amplitude equation

We previously saw that the unstable state is associated with a wave vector q_0 (being the first wave number to grow at the onset of instability $\epsilon = 0$). However, in reality, the system cannot be tuned precisely to this case, thus, at the onset of instability $\epsilon << 1$, a finite interval, close to q_0 will have an exponential growth in time ($\sigma(q) > 0$). What happens as all these modes grow can be investigated using the Amplitude equation formalism and be easily understood by analogy to the beating and modulation of two cosine functions with close wave numbers. The superposition of oscillations with similar frequencies leads to a "beating" in the overall amplitude. For a pattern forming system, this means that the strength of the pattern (the amplitude) varies much more slowly than the pattern itself.

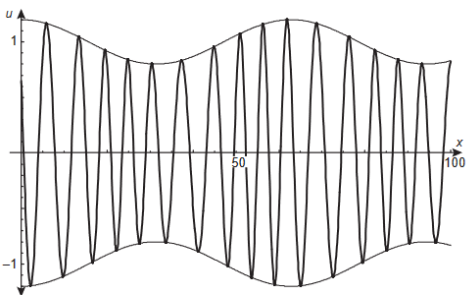

Figure 4: Example of a parametric plot $(\sin(x), \cos(x), x)$

Near onset $\epsilon << 1$, we separate fast and slow variables of space and time by introducing:

$$X = \epsilon^{1/2}x, \quad Y = \epsilon^{1/4}y, \quad T = \epsilon t \tag{21}$$

Expanding, $\psi = \epsilon^{1/2}\psi_0 + \epsilon\psi_1 + \dots$, at the lowest order we must satisfy:

$$\left(\partial_x^2 + q_0^2\right)^2 \psi_0 = 0 \quad \Rightarrow \quad \psi_0(x,t) = A(X,Y,T)e^{iq_0x} + \cdots \tag{22}$$

Solvability conditions lead to :

$$\tau_0 \partial_t A = \epsilon A + \xi_0 \left[\partial_x - (i/2q_0)\partial_y^2\right]^2 A - g_0|A|^2 A \tag{23}$$

Which is the amplitude equation that describes the evolution in space and time of the slow modulations of the base solution ψ_0. This allows us to see the *Ginzburg-Landau*XX equation as amplitude equation for the single Swift–Hohenberg equation XX.

4.3 The variational formulation of Swift-Hohenberg equation

One can observe that *Swift-Hohenberg* equation has a variational structure. It means that it possesses a *Lyapunov* functional $\mathcal{F}$, known as SH free energy:

$$\partial_t = \psi = -\frac{\delta \mathcal{F}}{\delta \psi} \quad \text{With} \quad \mathcal{F}[\psi] = \int \boldsymbol{dx}\, f(\psi, \nabla^2\psi) = \int \boldsymbol{dx} \left[-\frac{\epsilon}{2}\psi^2 + \frac{1}{2}\left(\nabla^2 + q_0^2\right)^2 \psi^2 + \frac{1}{4}\psi^4\right] \tag{24}$$

With f being a free energy density. The time derivative of the free energy can be written as:

$$\frac{d\mathcal{F}}{dt} = \int \boldsymbol{dx} \left\{-\epsilon\dot{\psi}\psi + \left[\left(\nabla^2 + q_0^2\right)^2 \psi\right]\dot{\psi} + \psi^3\dot{\psi}\right\} = -\int \left(\frac{\partial \psi}{\partial t}\right)^2 \boldsymbol{dx} \leq 0 \tag{25}$$

Hence, $\mathcal{F}$ is a decreasing "energy" through the evolution of the system. The dynamics is "downhill" and is sometimes called gradient flow. In addition, the final states can be obtained by finding minima of $\mathcal{F}$.

4.4 The concept of order parameter

Rayleigh-Bénard convection patterns are just one example of non-equilibrium pattern formation, a phenomenon seen across multiple and diverse systems. Experimental and theoretical studies suggest that similar pattern formation processes occur universally across these systems, indicating that spontaneous pattern formation in non-equilibrium systems can be described by the same mathematical tools, regardless of their specific characteristics.
This universality can be understood through the concept of *Order parameter*. Analysis shows that order parameters, governed by nonlinear partial differential equations, dictate the spatial and temporal evolution of patterns in various systems. Remarkably, systems as different as reaction-diffusion models and convection experiments exhibit the same underlying order parameter dynamics. This concept is particularly valid for systems near instabilities, where patterns emerge predictably from the system's fundamental mathematical structure. Consider some arbitrary pattern formation system described by a state vector $\boldsymbol{q}(\boldsymbol{r}, t)$, it obeys some partial differential equation:

$$\partial_t \boldsymbol{q} = \Theta[\boldsymbol{q}(\boldsymbol{r}, t)] \tag{26}$$

Where Θ is some differential operator. The long term behavior of $\boldsymbol{q}(\boldsymbol{r}, t)$, can be captured by an order parameter ψ, linked with $\boldsymbol{q}$ and it can be directly related to some easily observable physical quantity. The validity of the order parameter concept can be proved for systems close to instabilities, where the system's behavior changes qualitatively. The order parameter in the case of *Rayleigh-Bérnard* convection is the temperature field (or vertical velocity), it is the magnetization vector in the case of ferromagnets, or even an indicator function of the different phases in *Cahn-Hilliard* model, or damaged/undamaged materials in Gradient-damage facture models. An order parameter equation generally reads:

$$\partial_t \psi = h[\psi(\boldsymbol{r}, t)] \tag{27}$$

4.5 Topological defects in SH and PFC models

The equilibrium and dynamics of defects, in a small scale, plays in important role in the studies of the evolution of complex systems at different scales (Angheluta et al., 2012). Their statistical properties have a huge impact on the evolution of system, examples are given in quenching dynamics during phase ordering kinetics, defects in convection pattern, and dislocation dynamics in crystal plasticity. The emergence of topological defects is a common phenomena is systems supporting a continuous symmetry that is spontaneously broken during non-equilibrium phase transitions (Angheluta et al., 2012).
The topological theory of defects, as formalized by (Mermin, 1979), gives an elegant and precise language to understand the formation of defects. In fact, defects aries whenever the order parameter manifold is not simply connected, i.e it has a non trivial fundamental group π_0 (Pismen, 1999). The equilibrium properties of defects and their link with topological properties was heavily studied in (Pismen, 1999). The formulation and evolution of topological defects is formulated, typically, through the complex *Ginzburg-Landau* equation, where defect are described as phase singularities (The phase evolving in the circle $\mathcal{S}^1$, with non trivial homotopy group $\pi_0 \simeq \mathbb{Z}$).
The impact of dislocations on melting of solids was extensively studies in the 80's. The order liquid-crystal films was studied in (Toner & Nelson, 1981) (Nelson & Toner, 1981) while focusing the effect of dislocations and thermal fluctuations. In the same year, *Siggia* and *Zippelius* studied the dynamics of defects in *Rayleigh-Bérnard* convection using the gradient flow of the complex amplitude (Siggia & Zippelius, 1981). Later one, the *Swift-Hohenberg* model was used to study motion of isolated dislocations in Rayleigh-bernard roll structure (Shiwa & Kawasaki, 1986). *Halperin* introduced an analytical method of locating and tracking defects using Dirac's delta function δ (Halperin, 1981). Further more, this method was extended by *Mazenko* (Mazenko & Wickham, 1998) to excplicitly determine the velocities of topological defects. The idea behind the formalism is that in the "real space", let's say of dimension d, topological defects of a $d-$dimensional order parameter given as a vector field $\boldsymbol{\psi}(r) = \{\psi_\alpha(r)\}_{1\leq\alpha\leq n}$, are located at the zeros of the vector field. In fact, the "orientation" $\boldsymbol{\psi}/||\boldsymbol{\psi}||$, is well defined everywhere iff $\psi \neq 0$. So that the defects, i.e points where no orientation can be determined, are located by the zeros of $\boldsymbol{\psi}$; in other words, whenever $\delta(\boldsymbol{\psi}) = 1$. This definition holds in the space of $\boldsymbol{\psi}$, also known as the order parameter's manifold. In order to locate defects in the real space, we introduce the jacobian $\mathcal{D}$ of the variable transformation from the real space position $\vec{\boldsymbol{r}}$ to the order parameter manifold $\boldsymbol{\psi}$. Thus, we define a defect density $\rho_d(\boldsymbol{r})$(Halperin, 1981), in the real space, as :

$$\rho_d(\boldsymbol{r}, t) = \delta(\psi)\mathcal{D}(\boldsymbol{r}, t) = \sum_i q_i \delta(\boldsymbol{r} - \boldsymbol{r_i}) \tag{28}$$

This formula establishes the link between the distribution of defects located at position $\boldsymbol{r_i}$ having a topological charge $q_i = \mathcal{D}(\boldsymbol{r_i}, t)/||\mathcal{D}(\boldsymbol{r_i}, t)||$ to the zeros of the $d-$dimensional order parameter ψ. Note that when writing $\rho_d(\boldsymbol{r}, t) = \delta(\psi)\mathcal{D}(\boldsymbol{r}, t)$, the time dependence is only in $\mathcal{D}$, that's is to say the order parameter's manifold isn't changing it's the map from real space to it that's changing and carrying the time evolution information of the topological charges. In order to illustrate the previous equation, let's specialize for example to the case where $d = 2$ and the order parameter is complex number, let's say $\psi = (\psi_1, \psi_2)$ i.e $n = 2$. The orientation (phase) of ψ vanishes only in a set of separated point $\vec{r_i}$. The jacobian $\mathcal{D}(r)$ is a scalar quantity (Angheluta et al., 2012):

$$\mathcal{D}(r) = \begin{vmatrix} \partial_x\psi_1 & \partial_y\psi_1 \\ \partial_x\psi_2 & \partial_y\psi_2 \end{vmatrix} = \partial_x\psi_1\partial_y\psi_2 - \partial_y\psi_1\partial_x\psi_2 = \frac{1}{2i}\left\{\partial_x\psi^*\partial_y\psi - \partial_x\psi\partial_y\psi^*\right\} \tag{29}$$

The case where $d > n$ is more subtle to treat since jacobian of the transformation $\vec{r} \mapsto \psi(\vec{r})$ is not a square matrix and a determinant cannot computed. The orientation of the field can vanish on spaces * of higher dimensions. The example of $d = n + 1$ was treated in (Halperin, 1981) introduce codimension

and further detailed in (Mazenko, 1999) to explicity compute velocities. In this case defects are lines, with line density given, in terms of its components, by:

$$\rho_\alpha = \delta(\psi)\mathcal{D}_\alpha(r) \quad \text{with} \quad \mathcal{D}_\alpha = \frac{1}{n!}\epsilon_{\alpha i_2 \dots i_d}\epsilon_{j_1 j_2 \dots j_n}\partial_{i_2}\psi_{j_1}\partial_{i_3}\psi_{j_2}\dots\partial_{i_d}\psi_{j_n} \quad , \quad 1 \leq \alpha \leq d \tag{30}$$

with $\epsilon_{\alpha i_2 \dots i_d}$ being the fully anti-symmetric *Levi-Civita* tensor of order d. The rather cumbersome notation of the previous equation can be made simple in the case where $d = 3$ and $n = 2$.

$$D_\alpha = \frac{1}{2}\epsilon_{\alpha jk}\epsilon_{lm}\partial_j\psi_l\partial_k\psi_m = \frac{1}{2}\epsilon_{\alpha jk}\left[\partial_j\psi_1\partial_k\psi_2 - \partial_j\psi_2\partial_k\psi_1\right] = \epsilon_{\alpha jk}\left(\partial_j\psi_1\partial_k\psi_2\right) \tag{31}$$

Because $\epsilon_{\alpha jk} = -\epsilon_{\alpha kj}$. So that the i-component of the tangent vector to the defect line at point $\boldsymbol{r}$ are given by $\rho_i(\boldsymbol{r}) = \delta(\psi)\epsilon_{ijk}\left(\partial_j\psi_1\partial_k\psi_2\right)$. In addition, *Mazenko* (Mazenko, 1997) derived an explicit relation giving the velocity of defects. Using the fact that the determinant is a conserved invariant satisfying a continuity equation, with a current $\boldsymbol{\mathcal{J}}^\psi$ we write, in the case of a point defect ($n = d = 2$):

$$\partial_t\mathcal{D} + \nabla\cdot\boldsymbol{\mathcal{J}}^\psi = 0 \quad \text{with} \quad \mathcal{J}^\psi_\alpha = -\frac{i\epsilon_{\alpha\beta}}{2}\left(\dot{\psi}\partial_\beta\psi^* - \dot{\psi}^*\partial_\beta\psi\right) \tag{32}$$

By taking the time derivative of $\rho(r) = \delta(\psi)\mathcal{D}(r)$ we get:

$$\begin{aligned}\partial_t\rho &= \partial_t(\delta(\psi))\mathcal{D} + \delta(\psi)\partial_t\mathcal{D} \\ &= \frac{\partial\delta}{\partial\psi}\dot{\psi}\mathcal{D} + \delta(\psi)\partial_t\mathcal{D} \\ &= \frac{\partial\delta}{\partial\psi}\dot{\psi}\mathcal{D} - \delta(\psi)\nabla\cdot\mathcal{J}^\psi \quad \text{(by the continuity law of } \mathcal{D})\end{aligned} \tag{33}$$

An algebraic manipulation allows us to re-write $\dot{\psi}\mathcal{D}$. In fact:

$$\mathcal{J}^\psi\cdot\nabla\psi = \begin{bmatrix} -\frac{i}{2}\left(\dot{\psi}\partial_y\psi^* - \dot{\psi}^*\partial_y\psi\right) \\ \frac{i}{2}\left(\dot{\psi}\partial_x\psi^* - \dot{\psi}^*\partial_x\psi\right)\end{bmatrix}\cdot\begin{bmatrix}\partial_x\psi \\ \partial_y\psi\end{bmatrix} = \frac{i}{2}\dot{\psi}\left(\partial_x\psi^*\partial_y\psi - \partial_x\psi\partial_y\psi^*\right) = -\dot{\psi}\mathcal{D} \tag{34}$$

Replacing in the time derivative of the density ρ:

$$\partial_t\rho = \frac{\partial\delta}{\partial\psi}\dot{\psi}\mathcal{D} - \delta(\psi)\nabla\cdot\mathcal{J}^\psi = -\frac{\partial\delta}{\partial\psi}\mathcal{J}^\psi\cdot\nabla\psi - \delta(\psi)\nabla\cdot\mathcal{J}^\psi = -\nabla\cdot(\delta(\psi)\mathcal{J}^\psi) = -\nabla\cdot(\rho\frac{\mathcal{J}^\psi}{\mathcal{D}}) \tag{35}$$

By identification with the classical form of density conservation ($\partial_t\rho + \nabla\cdot(\rho v) = 0$), we define point defect velocity (Mazenko, 1997) :

$$\boldsymbol{v} = \frac{1}{\mathcal{D}}\boldsymbol{\mathcal{J}}^\psi \tag{36}$$

The previous result yields a way of determining the velocity of point defects directly from the complex order parameter ψ. This result can be easily generalized to higher dimensions, as extensively detailed in (Mazenko, 1999). Within this work, we limit ourselves to case where $n = 2, d = 3$. The velocity a dislocation curve is given by:

$$\vec{v} = \frac{1}{2||\vec{\mathcal{D}}||^2}\left(\vec{\mathcal{D}}\times(\dot{\psi}^*\nabla\psi - \dot{\psi}\nabla\psi^*)\right) \tag{37}$$

Where $\vec{\mathcal{D}} = (\mathcal{D}_i)$, the vector of determinants as previously defined, because the jacobian of the transformation is not a square matrix and in this case the current is second order tensor $\mathcal{J}^\psi_{ij}$ (Mazenko, 1999).

This paradigm herein introduced applies only to multi-dimensional order parameters $\boldsymbol{\psi}(r) = \{\psi_\alpha(r)\}_{1\leq\alpha\leq n}$. It was extended in (Skaugen et al., 2018a)(Skogvoll, Angheluta, et al., 2022) to study the motion of dislocations in defect crystal with PFC-model using the amplitude expansion as we shall next. In 2023, a unified field theory generalizing the work of *Mazenko* was proposed (Skogvoll et al., 2023) in order to describe defects and non-linear fast excitations in different systems : Bose-Einstein condensates, active nematics and crystal lattices.

5 Phase Field crystal model

5.1 Introduction

The Phase Field Crystal (PFC) model was introduced in 2002 by *Elder* and *Grant* (Elder et al., 2002) in order to include elasticity in crystal growth. The Swift-Hohenberg free energy was used and they argued that the factor $(\nabla^2 + q_0^2)$ was the simplest way the include peaks in the resulting structure at q_0 wavelength, which emulates the emergence of periodic crystal structure. Crystalline pattern was the key ingredient to include elasticity in the crystal growth model (Elder & Grant, 2004). In the PFC model, the scalar field ψ is a local average density and hence it's integral over the domain was meant to remain conserved (mass conservation). Thus, using *Swift-Hohenberg* functional $\mathcal{F}_{sh}[\psi]$, the phase field crystal model uses conserved dynamics to derive the evolution equation of ψ:

$$\partial_t \psi = \nabla \cdot \left(\Gamma \nabla \frac{\delta \mathcal{F}_{sh}}{\delta \psi} \right) \quad \text{with} \quad \mathcal{F}_{sh}[\psi] = \int \boldsymbol{dx} \left[-\frac{\epsilon}{2}\psi^2 + \frac{1}{2}\left(\nabla^2 + q_0^2\right)^2 \psi^2 + \frac{1}{4}\psi^4 \right] \tag{38}$$

This functional is minimized by constant (liquid state), strip state and hexagonal (triangular state) which can be understood as crystalline state. Despite its simplicity, the PFC model gives respectable descriptions of elasticity, since it was used to derive elastic constants by calculating the change of energy under some applied deformation (Elder et al., 2002), It was also used to compute yield stress and model softening (Elder & Grant, 2004). In addition, it reproduces both *Read-Shockley* grain boundary energies and *Matthews* and *Blakeslee* misfit dislocation behavior during epitaxy (Elder et al., 2002), and can accurately model liquid-phase epitaxial growth (Elder & Grant, 2004). The PFC model has been used in numeral mechanical studies included fracture propagation (Elder et al., 2002), plasticity avalanche (Chan et al., 2010), and edge dislocation dynamics (Elder et al., 2007a).

Although originally phenomenologically motivated, the PFC model had been derived from classical density functional theory (Archer et al., 2019) (Wu & Karma, 2007). To go into details, DFT describes a system of N interacting particles at positions $\boldsymbol{r}_i$ by an average one variable particle density $\rho(\boldsymbol{r})$ (inspired by pioneering work of *Hohenberg* and *Kohn* in the context of Quantum mechanics in order to provide approximate solutions to the multi-body *Shrödinger* equation). In the ne canonical ensemble, the average density is simply given by an ensemble average $\langle \cdot \rangle$:

$$\rho(\boldsymbol{r}) = \left\langle \sum_{i=0}^{N} \delta(r - r_i) \right\rangle \tag{39}$$

According to the *Hohenberg-Kohn* principle, there exist a free energy functional $\Omega[\rho]$ minimized at equilibrium. This functional is linked to Helmholtz free energy $\mathcal{F}$ by a simple legendre transformation:

$$\Omega[\rho, \mu, T] = \mathcal{F}[\rho, T] - \mu \underbrace{\int \rho(r) dr}_{} = \mathcal{F}[\rho, T] - \mu N \tag{40}$$

In classical DFT calculations, Helmholtz free energy is decomposed into two main contribution, in the absence of any external field, so that we write:

$$\mathcal{F}[T, \rho] = \mathcal{F}_{id}[T, \rho] + \mathcal{F}_{ex}[T, \rho] \tag{41}$$

The functional $\mathcal{F}_{id}[T, \rho] = k_B T \int \rho(r) \left(\ln(\Lambda^3 \rho(r)) - 1 \right) dr$ corresponds to the free energy of an ideal gas with k_B being Boltzmann's constant and $\Lambda = h/\sqrt{m = 2mk_BT}$ de Broglie's wavelength. The second term $\mathcal{F}_{ex}[T, \rho]$ corresponds to the excess free energy (deviation from ideal gas) due to all correlations from all interactions between particles. This functional is not known

and is only approximated. For that, we perform a taylor expansion around a uniform reference state ρ_{ref}. If we denote $\Delta\rho = \rho(r) - \rho_{ref}$, Taylor expanding yields:

$$\mathcal{F}_{\text{exc}}[T,\rho] = \mathcal{F}^{(0)}_{\text{exc}}[\rho_{\text{ref}}] + \sum_{n=1}^{\infty} \int d\mathbf{r}_1 \cdots \int d\mathbf{r}_n \frac{1}{n!} \frac{\delta^n \mathcal{F}_{\text{exc}}[T,\rho(\mathbf{r})]}{\delta\rho(\mathbf{r}_1)\ldots\delta\rho(\mathbf{r}_n)}\bigg|_{\rho_{\text{ref}}} \prod_{i=1}^{n} \Delta\rho(\mathbf{r}_i) \tag{42}$$

Since we are interested in the derivatives of $\mathcal{F}$, we can neglect the 0-th order term and the first order term too, who turns one to be a constant due to the isotropy of the bulk fluid. If We truncate the previous equation at its second order, we write:

$$\begin{aligned} \mathcal{F}_{\text{exc}}[T,\rho] &= \frac{1}{2!} \iint \frac{\delta^2 \mathcal{F}_{\text{exc}}[T,\rho(\mathbf{r})]}{\delta\rho(\mathbf{r}_1)\delta\rho(\mathbf{r}_2)}\bigg|_{\rho_{\text{ref}}} \Delta\rho(\mathbf{r}_1)\Delta\rho(\mathbf{r}_2)\, d\mathbf{r}_1\, d\mathbf{r}_2 \\ &= -\frac{k_B T}{2} \iint C_2(\mathbf{r}_1 - \mathbf{r}_2)\Delta\rho(\mathbf{r}_1)\Delta\rho(\mathbf{r}_2)\, d\mathbf{r}_1\, d\mathbf{r}_2 \end{aligned} \tag{43}$$

Where $C_2(\mathbf{r}_1 - \mathbf{r}_2)$ is the pair correlation function, and is the key ingredient to fine tuning the phase field crystal to procuce some desired phase diagrams as we shall see next. With the basis of DFT established, the dynamics are described by the central equation of *dynamical density functional theory* (**DDFT**), the conserved dissipative dynamics is given by:

$$\partial_t \rho(\mathbf{r},t) = \nabla \cdot \left[(k_B T)^{-1} M(\rho) \nabla \frac{\delta \mathcal{F}}{\delta \rho} \right] \tag{44}$$

With $M(\rho)$ being the mobility.

The model originally introduced, in 2002, is unfortunately only able to produce uniform, stripes and hexagonal (triangular states) and a corresponding phase diagram was produced (Elder & Grant, 2004). This limitation was quickly noticed, and a minor modification by Alain Karma was considered in order to produce BCC structures in 2D (Wu & Karma, 2007). Shorty after, in 2007, the 2D phase diagram (with BCC structures) was extended to 3D (Jaatinen & Ala-Nissila, 2010).
From a classical density functional theory, it was possible to predict both fcc and hcp structures, but this result has never been successfully reproduced in the PFC community, because of the liquid correlation function C_2 used, that does not seem to contain enough information to determine the solid state crystal structure. In 2011, It was shown that the excess free energy, can be constructured to create an energy minimum for a desired periodic structure (Greenwood et al., 2011), so that progress has been made in the PFC community by considering phenomenological forms for the Fourier transform of the two-point correlation function $\hat{C}_2$, carefully designed to stabilize a target structure: triangular and square lattices in 2D, and bcc, fcc, hcp, and sc lattices in 3D. Then, Following the same direction, it was shown in 2013 that the PFC model can be tuned to reproduce all five bravais lattices in 2D (Mkhonta et al., 2013).

5.2 Time scale in PFC

The fundamental time scale involved in phase field crystal is the diffusion time (Elder & Grant, 2004), because the model averages over rapid fluctuations in time to give a time scale of evolution on the order of diffusion rather than atomic vibration. To see that, consider a perfect equilibrium configuration ψ_{eq} of the original PFC model. Then, suppose that one particle is removed to create a vacancy in the lattice. Atomic vibrations will cause neighboring atom to hop into the vacancy so that the this defect will diffuse throughout the lattice. However, the vibration are integrated out in the PFC model and the all that is left is diffusion. In this sense, and from a phase field point of view, the density at the missing spot will gradually increase as the density at neighboring sites slowly decreases.

However, there are many phenomena, of important physical interest, that exist between the time scale of atomic vibration and the diffusive time scale (Stefanovic et al., 2006). But due to the dissipative dynamics of diffusing the scalar field, PFC model cannot model for example elastic interactions or fast dynamics (Heinonen et al., 2016). In a first attempt, *Stefanovic* proposed a *modified phase field crystal* (**MPFC**) model able to transmit short wavelength density fluctuation up to a time scale t_w after which the evolution continues diffusely (Stefanovic et al., 2006), but failed to describe large scale vibrations and couldn't reproduce correct phonon dispersion curves as noticed by (Majaniemi & Grant, 2007),(Majaniemi et al., 2008). The MPFC relies on including a second derivative, to add a wave-mode, in the time evolution equation of the scalar field ψ, it reads :

$$\frac{\partial^2 \psi}{\partial t^2} + \beta \frac{\partial \psi}{\partial t} = \alpha^2 \nabla^2 \frac{\delta \mathcal{F}}{\delta \psi} \tag{45}$$

In most up-to-date research, the phase field ψ is interpreted as a mass density, so that lattice distortion and mass variations are described by the same scalar, that evolves diffusively which is not physical. These two quantities, i.e mass and displacement should be considered independently (Acharya et al., 2022). This difficulty, along with including dissipation at a macroscopic scale remained unclear in challenging. *Heinonen* in 2016, formulated a complete hydrodynamic-PFC model which couples fast dynamics to dissipative processes on a mesoscopic length scale (Heinonen et al., 2016). He introduced a mesoscopic mass velocity v, and mass density ρ. The mass displacement, and lattice displacement are now subject to independent variations. Evolution equations were obtained by coarse graining (Athreya et al., 2006) the mass density and velocity fields by using the amplitude expansion framework and adding a dissipative *Navier-stokes* term. This model accurately describes fast dynamics but can be computationally expansive, especially if the mechanical relaxation happens several order of magnitudes faster than diffusion and plastic flows. Alternatively, an approach based on interpolation was proposed in (W. Zhou et al., 2019), in which the linear elastic displacement field was used to interpolate between grid points in order to ensure mechanical equilibrium but it was only valid for uniaxial loadings. A more recent work (Skaugen et al., 2018b), used the fact that the phase field crystal gives a good description of the incompatible part of mechanical stress so that it was supplmented by a smooth displacement field u^δ to ensure mechanical equilibrium $\psi(\boldsymbol{r}) \rightarrow \psi(\boldsymbol{r} - \boldsymbol{u}^\delta)$. This approach, later known as **MEqPFC**, was applied to the *amplitude phase field crystal* **APFC** to give a better computational approach to large systems (Salvalaglio et al., 2020).

Another path was the idea of scale separation using fourier filters as introduced in (Tóth et al., 2013), so that the dissipation of velocity was handled in the long rage limit but this model, as originally proposed, lacked the classical dissipation of the PFC model. This was introduced, along with fourier filters in (Podmaniczky & Gránásy, 2021) as a phenomenological damping parameter.
More recently, *Skogvoll* in 2022, suggested a consistent derivation of a coupling between PFC dynamics and a macroscopic velocity field (Skogvoll, Salvalaglio, & Angheluta, 2022). The separation of scales is done by means of fourier filers, just like (Tóth et al., 2013). Nonetheless, it is more versatile than the model suggested in (Heinonen et al., 2016) since it remains valid for large deformation too.

5.3 Dislocation dynamics with the PFC model

As previously seen, the phase field crystal model (PFC) was introduced as mesoscale description of crystalline solids. Since defects naturally emerge and evolve in the PFC model without any imposed rules, it was heavily used to study dislocations at the atomistic level (Berry et al., 2006)(Elder et al., 2007b)(Chan et al., 2010). However, a mesoscale model that bridges the atomic description with the macroscale continuum theory of mechanics and crystal plasticity (induced by the motion of dislocations) was still lacking.
In 2018, a first attempt was proposed to develop a theoretical framework to study plastic flow

(on a large scale) due to dislocation motion (on a small scale) (Skaugen et al., 2018a). The authors derived the configurational elastic stress by analyzing variations in the free energy under weak distortions:

$$\sigma_{ij}^{\psi} = [\partial_i \mathcal{L}\psi]\partial_j\psi - [\mathcal{L}\psi]\partial_{ij}\psi - f\delta_{ij} \tag{46}$$

Furthermore, they then linked the classical Burgers vector density to field singularities using the *Mazenko-Halperin* method (Halperin, 1981)(Mazenko, 1997). The phase-field crystal (PFC) model, which is based on the *Swift-Hohenberg* framework, uses a smooth, non-singular scalar field for the order parameter ψ, which inherently limits its ability to capture defects. However, close to the bifurcation point, an amplitude expansion is applicable, allowing complex amplitudes A_n to be used to identify defect locations (by tracking the zeros of A_n) and explicitly determine their velocities. Under specific assumptions, the authors also derived an expression that relates the velocity of dislocations to the average elastic stress (as determined from the phase field)(Skaugen et al., 2018a). This expression aligns with the classical *Peach-Koehler* force and provides an explicit form for the mobility coefficient. They validated their theory by examining the pure climb and pure glide of a dislocation dipole within a hexagonal lattice, observing that dislocations moved until they annihilated, which aligns with expected physical behavior. Furthermore, the authors compared the average elastic stress $\langle\sigma_{ij}^{\psi}\rangle$ obtained from the PFC model with classical elasticity solutions. They found good agreement between the two approaches, except within the dislocation core region. When comparing the tracked velocities to those predicted by the Peach-Koehler force, they observed a clear and significant discrepancy, which goes back to the fact that the mechanical information (σ_{ij}^{ψ}) encoded in the phase field is irrelevant. The model was evolving dislocations outside a mechanically equilibrated setting.

As long as the phase field ψ, that evolves diffusively, is interpreted as a mass density, mechanical equilibrium cannot be assured. Plastic motion is slow on the scale of lattice variation and happens at mechanical equilibrium. However, any non equilibrium deformation of ψ will only evolve diffusively which is unphysical. An attempt at detaching mass motion and lattice distortion was then proposed in (Skaugen et al., 2018b), by explicitly accounting for the separation of elastic and plastic time scales. They retain the PFC model since it acts a reliable tool to locate and track defects, and they supplement it with a smooth distortion field u^{δ} to ensure mechanical equilibrium. In fact, the phase field only gives the incompatible part of the stress σ_{ij}^{ψ} to which they add another smooth contribution to ensure that equilibrium is preserved.

$$\sigma_{ij} = \sigma_{ij}^{\psi} + \sigma_{ij}^{\delta} = \sigma_{ij}^{\psi} + \lambda\delta_{ij}u_{kk}^{\delta} + 2\mu u_{ij}^{\delta} \tag{47}$$

The smooth field u^{δ} has no impact on dislocation density (since the latter is defined as curl), and it is used to displace the field at each time step $\Delta t : \psi(\boldsymbol{r}) \rightarrow \psi(\boldsymbol{r} + \boldsymbol{u}^{\delta})$. Conveniently, this additional field serves as straightforward way to implement boundary conditions when solving for u^{δ} using Airy's stress function χ in a more computationally performant than the penalty term $M(x,y)(\psi - \psi_{trac})^2$ classically used to apply axial strain introduced (Stefanovic et al., 2009). As a benchmark of their mechanically equilibrated PFC theory (Skaugen et al., 2018b), the authors studied annihilation of a dislocation dipole in glide condition. The model gave a velocity that agrees with the classical theory, and regularized stresses that agreed with the linear elasticity solutions far for the core (the classical solution diverges in the core). This approach, known as **MEqPFC**, was also applied in the amplitude phase field crystal model for better computational approach in large systems (Salvalaglio et al., 2020). The fact that dislocations give rise to lattice incompatibilities and that the phase field ψ is a good descriptor of the incompatible stress, it seems only natural to use the incompatible strain in order to study dislocation nucleation. Authors in (Skogvoll et al., 2021) introduced a incompatibility field η^{ψ}:

$$\eta^{\psi} = \frac{1}{2\mu}\left(\epsilon_{ik}\epsilon_{jl}\partial_i\sigma_{kl}^{\psi} - \kappa\nabla^2\sigma_{kk}^{\psi}\right). \tag{48}$$

They showed that the incompatibility field can accurately be used to diagnose dislocation nucleation. In fact, the location of the maximum $\max \eta^{\psi}$ gives an indicator of where the nucleation dipole will appear and the symmetry of η^{ψ} prior to nucleation yields the Burgers vector direction. Following this work, a full theory of the Kinematics of dislocation lines in three-dimensional anisotropic crystal solids was proposed in (Skogvoll, Angheluta, et al., 2022). The authors applied it to study dislocation loops and showed that the motion is driven by a Peach-Koehler like force and it gives stresses that agree with classical solutions in the far field. Even more recently, *Skogvoll* (Skogvoll, Salvalaglio, & Angheluta, 2022) suggested a a complete and general coupling of hydrodynamics and phase field crystal able to couple the diffusive evolution of the scalar field with the fast dynamics of a macroscopic velocity field, using coarse-graining. It was shown that the resulting model is able to the evolve the PFC at mechanical equilibrium. The authors argued that the model is general an can used to study large deformations and dynamics since it captures elastic waves properly.

6 Field dislocation mechanics and phase field crystal

It was already pointed out before that the main shortcoming of the phase field crystal is that scalar field ψ is interpreted as a mass density so that lattice and mass do not independent variations. Their evolution is bound the disspative diffusion of the scalar field $\partial_t \psi = \Gamma \nabla^2 (\delta \mathcal{F} / \delta \psi)$, which cannot ensure correct mechanical equilibrium since it cannot replicate lattice relaxations in phonon mode. We previously introduced the approaches that were suggest in order to ensure mechanical equilibrium and account for the different timescales involved in bridging scales in dislocations-mediated crystal plasticity. However, other questions remained open namely on how to accurately consider imposed tractions and displacements on the boundary, how to account for shape-changing domains, and how to correctly handle the reversible processes of converting a macroscopic mechanical work to elastic energy in a purely dissipative theory.

The approach we take here is somewhat different from the previous works in the field and is based on the coupling between field dislocation mechanics and phase field crystal as proposed in (Acharya & Viñals, 2020). The tenet of theory is considering as independent the following variables : the phase field ψ, the mass velocity v, the elastic distortion W and the mass density ρ. Such separation is achieved via postulating a free energy of the form :

$$\mathcal{F}[\rho, \boldsymbol{W}, \psi] = \int_{\Omega} \rho \varphi_e(\rho, \boldsymbol{W}, \psi, \boldsymbol{P})\, dx + C_{sh} \Phi_{sh}[\psi] + \frac{C_W}{2} \int \rho |\boldsymbol{W} - \boldsymbol{P}|^2\, dx + \frac{C_\rho}{2} \int \rho (\rho - \psi)^2\, dx \tag{49}$$

A key element of theory is the introduction of a second order tensor $\boldsymbol{P}$ called local configurational tensor. It is a functional of the scalar field $\boldsymbol{P}[\psi]$ that maps at each point the distorted wave vectors $\boldsymbol{q}^n$ to the ground state undistorted ones $\boldsymbol{q}_0^n$:

$$\boldsymbol{q}_0^n = \boldsymbol{P}^{-T} \boldsymbol{q}^n \tag{50}$$

The first term in the free energy introduced in eq. (49) is the classical elastic energy but to which we add an explicit dependence on the crystalline order parameter ψ and the defect induced distortion indicated by P. This is due to the fact that the elastic tensor will depend the crystal symmetry and will depend on the local state of distortion. The second term is the classical Swift-Hohenberg energy to enforce periodicity in the ground state and include and non convex term in the total free energy of the system. The third term is a penalization of the difference between the inverse elastic distortion and the phase field configurational distortion. The last term is a penalization of of the difference between mass density and the phase field. It is however important to note here that the phase field ψ is not interpreted as mass density and is not a conserved quantity as we shall see next. The role of the phase field in this model is mainly to incorporate non convexity in the free energy so that a crystalline structure is considered even if

locally deformed. It also serves us to locate defects track them and ensure the conservation of topological charges during motion. It is important to highlight that the free energy functional introduced in eq. (49) exhibits a clear separation between elastic energy φ_e and swift-Hohenberg one Φ_{sh}, the scalar field ψ has no contribution whatsoever to the elastic deformation.

The model includes three coupling constants C_{sh}, C_W and C_ρ that are positive and must be tuned to justify a physically correct model of mechanically stressed crystalline solids. Bounds of the coupling constants must be sought and these bounds will give insights onto the relative times scales of elastic and plastic motion.

The set of governing equations is as follows:

$$
\begin{aligned}
\text{Mass conservation :} \quad & \dot{\rho} + \rho \operatorname{div} \boldsymbol{v} = 0 \\
\text{Momentum conservation :} \quad & \rho \dot{\boldsymbol{v}} = \mathbf{div}\, \boldsymbol{T} + \rho \boldsymbol{b} \\
\text{Topological charge :} \quad & \mathbf{curl}\, \boldsymbol{W} = \mathbf{curl}\, \boldsymbol{P} = -\boldsymbol{\alpha} \quad , \quad \dot{\boldsymbol{W}} + \boldsymbol{W}\boldsymbol{L} = \boldsymbol{\alpha} \times \boldsymbol{V}^d \\
\text{Symmetric reversible stress :} \quad & \boldsymbol{T} = -\rho \left[\boldsymbol{W}^T \left(\frac{\partial \varphi_e}{\partial \boldsymbol{W}} + C_w \frac{\partial \varphi_{wp}}{\partial \boldsymbol{W}} \right) + \boldsymbol{P}^T \left(\frac{\partial \varphi_e}{\partial \boldsymbol{P}} + C_w \frac{\partial \varphi_{wp}}{\partial \boldsymbol{P}} \right) + a \boldsymbol{I} \right]_{sym} \\
\text{Dislocations velocity :} \quad & \boldsymbol{V}^d = -M \boldsymbol{\mathcal{E}} : \left[\rho \left(\frac{\partial \varphi_e}{\partial \boldsymbol{W}} + C_w \frac{\partial \varphi_{wp}}{\partial \boldsymbol{W}} \right)^T \boldsymbol{\alpha} \right] \\
\text{Phase field evolution :} \quad & \dot{\psi} = -L \left[C_{sh} \frac{\delta \Phi_{sh}}{\delta \psi} + C_\rho \rho (\rho - \psi) + \frac{\delta \Phi_{wp}}{\delta \psi} \right]
\end{aligned}
$$

Where we used the following definitions:

$$
\varphi_{wp} = \frac{1}{2} |\, \boldsymbol{W} - \boldsymbol{P}|^2 \quad \text{and} \quad \Phi_{wp} = \int_\Omega \rho \varphi_e \boldsymbol{dx} + C_w \int_\Omega \rho \varphi_{wp} \boldsymbol{dx}
$$

More recently, a weak one way coupling between FDM and PFC was proposed (Upadhyay & Viñals, 2024). The authors use the phase field ψ to locale dislocations and compute a configurational elastic distortion $\boldsymbol{Q}$, the later is used to extract the phase field dislocation tensor $\overline{\boldsymbol{\alpha}}$. The one way weak coupling consists in setting the FDM dislocation density tensor $\boldsymbol{\alpha}$ equal to $\overline{\boldsymbol{\alpha}}$, which implies that the incompatible part of the elastic distortion $\boldsymbol{U}^\perp$ is equal to the incompatible part of $\boldsymbol{Q}$, and the compatible part $\boldsymbol{U}^\parallel$ should be sought to ensure mechanical equilibrium. The authors studied a stationary dislocation dipole under periodic boundary conditions, and solved the involved equation via spectral methods. Their main finding was local relaxation of the order parameter near the core is fast and thus elastic equilibrium is quickly established (U doesn't evolve from $t = 5$). However, the configurational distortion $\boldsymbol{Q}$ continues to evolve until $t = 20000$ to reach a steady state (due the diffusive evolution of ψ), which is unphysical and limits the mechanical applications of PFC model. Additionally, They compared configurational stress directly extracted from the phase field $\boldsymbol{\sigma}^\psi$, the configurational stress $\boldsymbol{\sigma}^Q$ with the elastic FDM solution $\boldsymbol{\sigma}$. Initially, the stresses differ as excepted. However, when steady state is reached, they all match in the far field (up to some slight differences). The main deviations are found within dislocation cores, and its due the fact that the elastic solution is linear and derived from static FDM whereas the PFC stress is derived from non linear free energy which can be thought of as a regularization.

It must be have become clear at this point that the *phase field crystal* **PFC** is a consistent and promising method to include defects in the continuum mechanics. However, a fully coupled model was never investigated previously and we shall seek in this work wether the proposed theory proposed in (Acharya & Viñals, 2020) provides an improved framework for the description of dislocation-mediated plasticity in metals.

7 Kinematics of Burgers vector conservation

7.1 Dislocation transport equation

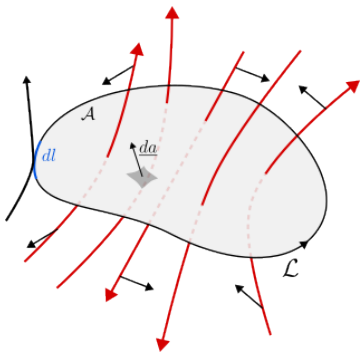

(a) A bundle of dislocation lines threading through a patch $\mathcal{A}$, delimited by a closed curve $\mathcal{L}$.

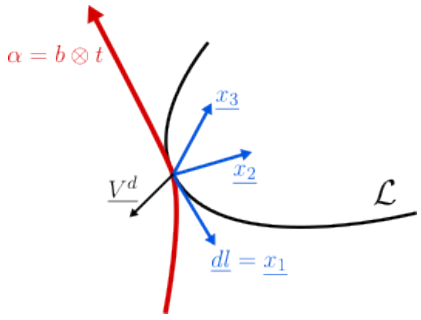

(b) A local frame analysis of a dislocation line crossing the boundary $\mathcal{L}$ with velocity $\boldsymbol{V}^d$.

Figure 5: Illustration of Burgers vector transport through a patch $\mathcal{A}$

The idea behind Burgers vector conservation, in the case of moving dislocations is to introduce a balance law of the type:

Rate of change = what comes in - what comes out

For that, we consider an area patch $\mathcal{A}$, delimited by a closed curve $\mathcal{L}$. The Burgers vector content can be thought of as bundle of lines each carrying a given Burgers vector $\boldsymbol{b}$ entering or exiting the surface $\mathcal{A}$, see fig. 5a. As dislocations move with a velocity field $\boldsymbol{v}^d$, the rate of change of the Burgers vector content is given as follows:

$$\frac{\partial}{\partial t}\left[\int_{\mathcal{A}(t)} \boldsymbol{\alpha}\,\boldsymbol{n}\,da\right] \tag{51}$$

Note that the integration is performed over an evolving area $\mathcal{A}(t)$ (so it its boundary $\mathcal{L}(t)$).
The main conceptual idea is that since the Burgers vector is constant along each individual dislocation line, how dislocation lines evolve within the patch does not matter and does not affect the rate of the change of dislocations content. What really contributes is the Burgers information crossing the contour $\mathcal{L}(t)$, i.e leaving or entering the patch $\mathcal{A}(t)$. For that we have to integrate, along the closed curve, elementary contributions on each infinitesimal element $\boldsymbol{dl}$. This contribution should extract only the Burgers vector content that crossed the element and left/entered the area. If we denote by f the flux of Burgers vector crossing an element $\boldsymbol{dl}$ along $\mathcal{L}$, then the conservation law of Burgers content becomes:

$$\frac{\partial}{\partial t}\left[\int_{\mathcal{A}(t)} \boldsymbol{\alpha}\,\boldsymbol{da}\right] = \oint_{\mathcal{L}(t)} f\,\boldsymbol{dl} \tag{52}$$

At this step, Burgers vector flux f can be either a scalar or a second order tensor so that the R.H.S of the previous equation yields a vector to be integrated over the closed curve.

A local analysis in a simple case of this statement comes as following:
Consider an infinitesimal curve element $\boldsymbol{dl}$, crossed by a dislocation line with tangent vector $\boldsymbol{t}$ and carrying a Burgers vector $\boldsymbol{b}$, see fig. 5b . The dislocation line moves with a velocity $\boldsymbol{v}^d$ with respect to the material. Clearly, if $\boldsymbol{v}^d$ is parallel to $\boldsymbol{t}$, no flux is generated, because $\boldsymbol{b}$ is constant along the dislocation line and the line doesn't end within the body. Also, obviously if $\boldsymbol{v}^d$ is

parallel $\boldsymbol{dl}$, no flux is generated, because nothing leaves the patch $\mathcal{A}$.

$\Rightarrow$ This means that Brugers flux is generated iff $\boldsymbol{v^d}$ is perpendicular to both $\boldsymbol{t}$ and $\boldsymbol{dl}$. Or in other words, only perpendicular components of $\boldsymbol{v^d}$ to both vectors generate some Burgers flux.

Mathematically, this is performed using mixed product $\boldsymbol{v^d} \cdot (\boldsymbol{t} \times \boldsymbol{dl})$, which projects the velocity $\boldsymbol{v^d}$ on the normal vector $\boldsymbol{t} \times \boldsymbol{dl}$. To exhibit $\boldsymbol{dl}$, we use the circular shift of triple product:

$$\boldsymbol{v^d} \cdot (\boldsymbol{t} \times \boldsymbol{dl}) = (\boldsymbol{v^d} \times \boldsymbol{t}) \cdot \boldsymbol{d_l} = -(\boldsymbol{t} \times \boldsymbol{v^d}) \cdot \boldsymbol{d_l} \tag{53}$$

This motivates the tensorial form of the previous statement in order to incorporate all possible directions crossing $\boldsymbol{dl}$. We define the dislocation density flux tensor as :

$$\boldsymbol{f} = -\boldsymbol{\alpha} \times \boldsymbol{v^d} \tag{54}$$

Let's stop for a moment to understand the cross product between a second order tensor and vector field. In fact, the quantity $\boldsymbol{\alpha} \times \boldsymbol{v^d}$ is a new second order tensor whose lines are vectors given by the cross product of each line of the $\boldsymbol{\alpha}$ in it matrix form with the vector field $\boldsymbol{v^d}$. This is best seen in indicial notation:

$$\boldsymbol{\alpha} \times \boldsymbol{v^d} = \underbrace{\boldsymbol{\mathcal{E}_{jkl}} \alpha_{ik} v_l^d}_{([\boldsymbol{\alpha}]^i \times \boldsymbol{v^d}) \cdot \hat{\boldsymbol{e_i}}} \hat{\boldsymbol{e_i}} \otimes \hat{\boldsymbol{e_j}} \tag{55}$$

Where, $[\alpha]^i$ is meant to represent line i in matrix' representation of $\boldsymbol{\alpha}$. Intuitively, a line i in represents, crudely, all components of tangent vectors whose corresponding burgers vector is along $\hat{\boldsymbol{e_i}}$. In this optic, the Burgers flux density f previously introduced will have a tensorial nature :

$$\boldsymbol{f} = -\boldsymbol{\alpha} \times \boldsymbol{v^d} \tag{56}$$

So that the RHS of eq. (52), will act as mixed product for all directions: each line of $\boldsymbol{\alpha}$ is crossed with $\boldsymbol{v^d}$ and then dotted with $\vec{dl}$ to extract normal components along each directions (these are the only contributions to any change in Burgers vector content). We write as (Acharya, 2011) (Appendix B):

$$\frac{\partial}{\partial t}\left[\int_{\mathcal{A}(t)} \boldsymbol{\alpha}\, \boldsymbol{da}\right] = -\oint_{\mathcal{L}(t)} \boldsymbol{\alpha} \times \boldsymbol{v^d}\, \boldsymbol{dl} \tag{57}$$

This derivation was influenced the discussion (Fressengeas, 2017). A different construction is suggested by (Mura, 1963), by (Fox, 1966) and by (Kosevich, 1965). We focus on the later in the following section.

7.2 Kosevich's construction

In his work (Kosevich, 1965), *Kosevich* argues that in the case of moving dislocations, the spatial gradient of the material velocity field $\partial v_k/\partial x_i$ and time derivative of the elastic distortion $\partial w_{ik}/\partial t$ are not equal (with $u_{ik} = \partial u_k/\partial x_i$). They are equal in the absence of dislocations. So in general, when dislocation are involved, we have:

$$\frac{\partial v_k}{\partial x_i} \neq \frac{\partial u_{ik}}{\partial t} \tag{58}$$

It is important to note here the similarity with the phase field crystal, if the same scalar field is used to describe mass He introduces a tensor field j_{ik} to balance these two quantities. He calls j_{ik} the dislocation flux density and He writes:

$$\frac{\partial u_{ik}}{\partial t} = \frac{\partial v_k}{\partial x_i} - j_{ik} \tag{59}$$

For compatibility reasons, he states that:

$$\partial_t \boldsymbol{\alpha} + \mathbf{curl}\, \boldsymbol{j} = 0 \tag{60}$$

He also shows that, at least, locally, a flux of Burgers vector is generated iff the velocity is perpendicular to both tangent to a curve and to the dislocation line:

$$j_{ik} = N\mathcal{E}_{ilm} t_l b_k V_m \quad \sim \boldsymbol{\alpha} \times \boldsymbol{v^d} \tag{61}$$

In addition, in his work, states that the total geometric distortion U_{ik} (and not the elastic distortion) is actually equal to the gradient of the velocity field .

$$\frac{\partial v_k}{\partial x_i} = \frac{\partial U_{ik}}{\partial t}$$

Replacing $\partial v_k / \partial x_i$ by 59, we write that:

$$\frac{\partial v_k}{\partial x_i} = \frac{\partial}{\partial t}\left(U_{ik} - u_{ik}\right) = \partial_t u^{pl}_{ik} \quad \text{with} \quad u^{pl} \equiv U - u \tag{62}$$

Which means that j_{ik} is linked to the rate of plastic distortion in the medium.

Acharya in 2011, in annex B, he restates the conservation of Burgers vector in case of a moving dislocation distribution. The localization of the conservation of Burgers vector yields two main results: An evolution law for $\boldsymbol{\alpha}$ and an additive decomposition of $\boldsymbol{L}$ which was only seen in his work in 2015.

7.3 Evolution law of dislocation density tensor :

Burgers vector balance law states that :

$$\frac{\partial}{\partial t}\left[\int_{\mathcal{A}(t)} \boldsymbol{\alpha}(\boldsymbol{x}, t)\, \boldsymbol{da}\right] = -\oint_{\mathcal{L}(t)} \boldsymbol{\alpha} \times \boldsymbol{v^d}\, \boldsymbol{dl} \tag{63}$$

Using Stokes-theorem, one can write :

$$\frac{\partial}{\partial t}\left[\int_{\mathcal{A}(t)} \boldsymbol{\alpha}(\boldsymbol{x}, t)\, \boldsymbol{da}\right] = -\int_{\mathcal{A}(t)} \mathbf{curl}\, \boldsymbol{\alpha} \times \boldsymbol{v^d}\, \boldsymbol{da} \tag{64}$$

7.3.1 Small deformations :

In the case of small deformations, one can assume that approximately $\mathcal{A}(t) \approx \mathcal{A}_0$ is invariant. The time derivative goes inside the integral and we get by localization theorem:

$$\dot{\boldsymbol{\alpha}} = -\mathbf{curl}\, \boldsymbol{\alpha} \times \boldsymbol{v^d} \tag{65}$$

Which yields the evolution law of the dislocation density $\boldsymbol{\alpha}(\boldsymbol{X}, t)$.

7.3.2 Finite deformations :

In the case of Finite deformations, the time derivative cannot be inverted with the integration operation since the domain is time variant. The remedy to this, is to pull-back everything to the initial (as-received) configuration using Nanson formula: $\boldsymbol{da} = J\boldsymbol{F}^{-t}\boldsymbol{dA}$ and the tranformation mapping $\varphi(\boldsymbol{X}, t)$

$$\frac{\partial}{\partial t}\left[\int_{\mathcal{A}_0} J\boldsymbol{\alpha}(\varphi(\boldsymbol{X}, t), t)\boldsymbol{F}^{-t}\, \boldsymbol{dA}\right] = -\int_{\mathcal{A}_0} J\mathbf{curl}\, \boldsymbol{\alpha} \times \boldsymbol{v^d}\, \boldsymbol{F}^{-t}\, \boldsymbol{dA}$$

Were, explicitly Highlight the fact that the fields depend on the Lagragian variable $\boldsymbol{X}$.
Inverting the integration and time derivation then localizing yields the following result:

$$\frac{\partial}{\partial t}\left[J\boldsymbol{\alpha}(\varphi\left(\boldsymbol{X},t\right),t)\boldsymbol{F}^{-t}\right]=-J\,\mathbf{curl}\left(\boldsymbol{\alpha}\times\boldsymbol{v}^{\boldsymbol{d}}\right)\boldsymbol{F}^{-t}$$

The LHS can be expanded :

$$\frac{\partial}{\partial t}\left[J\boldsymbol{\alpha}(\varphi\left(\boldsymbol{X},t\right),t)\boldsymbol{F}^{-t}\right]=\dot{J}\boldsymbol{\alpha}\,\boldsymbol{F}^{-t}+J\dot{\boldsymbol{\alpha}}\,\boldsymbol{F}^{-t}+J\boldsymbol{\alpha}\,\dot{\boldsymbol{F}^{-t}}=-J\,\mathbf{curl}\left(\boldsymbol{\alpha}\times\boldsymbol{v}^{\boldsymbol{d}}\right)\boldsymbol{F}^{-t}\tag{66}$$

where $\dot{\boldsymbol{\alpha}}$ is the material derivative.
Now, we investigate all time derivatives involved in the previous equation. The first terme involving $\dot{J}$, can be easily computed using the mass conservation laws: (recall that $\boldsymbol{x}=\varphi(\boldsymbol{X},t)$)

$$\text{Lagragian}:\rho_0(\boldsymbol{X})=J(\boldsymbol{X},t)\rho(\boldsymbol{x},t)\qquad\qquad\text{Eulerian}:\dot{\rho}+\rho\,\mathrm{div}\,\boldsymbol{v}=0$$

Derivating the Lagragian balance law and replacing $\dot{\rho}$ with its expression from the Eulerian law gives:

$$0=\dot{J}\rho+J\dot{\rho}\quad\Rightarrow\quad\boxed{\dot{J}=J\,\mathrm{div}\,\boldsymbol{v}=J\mathbf{Tr}\,L}\tag{67}$$

For the last term in 66, one easily obtains (Since transposition is commutative with derivation and inversion):

$$\boldsymbol{F}\,\boldsymbol{F}^{-1}=\boldsymbol{I}_3=\quad\Rightarrow\quad\underbrace{\dot{\boldsymbol{F}}\,\boldsymbol{F}^{-1}}_{=\boldsymbol{L}}+\boldsymbol{F}\,\dot{\boldsymbol{F}^{-1}}=0\quad\Rightarrow\quad\boxed{\dot{\boldsymbol{F}^{-t}}=-\boldsymbol{L}^{t}\boldsymbol{F}^{-t}}\tag{68}$$

With this two elements, we replace 68 and 67 in 66. Hence, we find:

$$\boxed{(\mathrm{div}\,\boldsymbol{v})\,\boldsymbol{\alpha}+\dot{\boldsymbol{\alpha}}-\boldsymbol{\alpha}\,\boldsymbol{L}^{\boldsymbol{t}}=-\mathbf{curl}\,\boldsymbol{\alpha}\times\boldsymbol{v}^{\boldsymbol{d}}}\tag{69}$$

Because $J=det\boldsymbol{F}\neq 0$.
We expand the material derivative:

$$\dot{\boldsymbol{\alpha}}=\partial_t\boldsymbol{\alpha}+(\mathbf{grad}\,\boldsymbol{\alpha})\cdot\boldsymbol{v}\tag{70}$$

The evolution law of the dislocation density tensor becomes:

$$\partial_t\boldsymbol{\alpha}+(\mathbf{grad}\,\boldsymbol{\alpha})\cdot\boldsymbol{v}+(\mathrm{div}\,\boldsymbol{v})\,\boldsymbol{\alpha}-\boldsymbol{\alpha}\,\boldsymbol{L}^{\boldsymbol{t}}=-\mathbf{curl}\,\boldsymbol{\alpha}\times\boldsymbol{v}^{\boldsymbol{d}}\tag{71}$$

A simple identity yields :

$$(\mathbf{grad}\,\boldsymbol{\alpha})\cdot\boldsymbol{v}+(\mathrm{div}\,\boldsymbol{v})\,\boldsymbol{\alpha}-\boldsymbol{\alpha}\,\boldsymbol{L}^{\boldsymbol{t}}=\mathbf{curl}\,\boldsymbol{\alpha}\times\boldsymbol{v}^{\boldsymbol{d}}\tag{72}$$

with can be easily proven in indicial notations:

$$\begin{aligned}\left[(\mathbf{grad}\,\boldsymbol{\alpha})\cdot\boldsymbol{v}+(\mathrm{div}\,\boldsymbol{v})\,\boldsymbol{\alpha}-\boldsymbol{\alpha}\,\boldsymbol{L}^{\boldsymbol{t}}\right]_{ij}&=\alpha_{ij,k}v_k+v_{k,k}\alpha_{ij}-\alpha_{ik}v_{j,k}\\&=(\alpha_{ij}v_k)_{,k}-(\alpha_{ik}v_j)_{,k}\quad\text{because}\quad\alpha_{ik,k}=0\quad(\mathbf{div}\;\boldsymbol{\alpha}=0)\end{aligned}$$

We note that, in components form:

$$\begin{aligned}[\mathbf{curl}\,\boldsymbol{\alpha}\times\boldsymbol{v}]_{ij}&=\mathcal{E}_{lkj}(\boldsymbol{\alpha}\times\boldsymbol{v})_{ik,l}\\&=\mathcal{E}_{lkj}(\alpha_{in}v_m\mathcal{E}_{nmk})_{,l}\\&=\mathcal{E}_{lkj}\mathcal{E}_{nmk}(\alpha_{in}v_m)_{,l}\\&=\mathcal{E}_{jlk}\mathcal{E}_{nmk}(\alpha_{in}v_m)_{,l}\\&=\left(\delta^j_n\delta^l_m-\delta^j_m\delta^l_n\right)(\alpha_{in}v_m)_{,l}\\&=\delta^j_n\delta^l_m(\alpha_{in}v_m)_{,l}-\delta^j_m\delta^l_n(\alpha_{in}v_m)_{,l}\\&=(\alpha_{ij}v_m)_{,m}-(\alpha_{il}v_j)_{,l}\end{aligned}$$

This proves THE IDENDITY :

$$(\mathbf{grad}\,\boldsymbol{\alpha})\cdot\boldsymbol{v}+(\operatorname{div}\boldsymbol{v})\,\boldsymbol{\alpha}-\boldsymbol{\alpha}\,\boldsymbol{L}^{t}=\mathbf{curl}\,\boldsymbol{\alpha}\times\boldsymbol{v} \tag{73}$$

Replacing 73 in 71, yields:

$$\boxed{\partial_t\boldsymbol{\alpha}+\mathbf{curl}\,(\boldsymbol{\alpha}\times(\boldsymbol{v}^{\boldsymbol{d}}+\boldsymbol{v}))=0} \tag{74}$$

7.3.3 Additive decomposition of velocity gradient tensor:

Another way to localize the Brugers vector balance law, would be to forumlate it in terms of the inverse elastic distortion $\boldsymbol{W}$. We recall that the dislocation density tensor $\boldsymbol{\alpha}$ is defined as:

$$\boldsymbol{\alpha}=-\mathbf{curl}\;\boldsymbol{W}$$

Replacin in Brugers vector Conservation Law 63, one finds :

$$\frac{\partial}{\partial t}\left[\int_{\mathcal{A}(t)}\mathbf{curl}\;\boldsymbol{W}\;\boldsymbol{da}\right]=\oint_{\mathcal{L}(t)}\boldsymbol{\alpha}\times\boldsymbol{v}^{\boldsymbol{d}}\;\boldsymbol{dl}\quad\xRightarrow[\text{Theorem}]{\text{Stokes}}\quad\frac{\partial}{\partial t}\left[\int_{\mathcal{L}(t)}\boldsymbol{W}\;\boldsymbol{dl}\right]=\oint_{\mathcal{L}(t)}\boldsymbol{\alpha}\times\boldsymbol{v}^{\boldsymbol{d}}\;\boldsymbol{dl}$$

One can can be tempted to pull back to the initial configuration, as previously done, but $\dot{\boldsymbol{W}}$ is ill defined on the initial configuration. As a remedy to this issue, Acharya 2004, suggests to fix an instant in time, say t, in which we wich to evalulat the quantities. Starting from time t, the motion is now parametrized by a new variable $\tau\in[t,+\infty[$. We denote by $\boldsymbol{F_\tau}$, the deformation gradient associated with the motion from t to $t+\tau$.
We evaluate the previous equation at time τ, and we explicitly write a τ subsccript to indicate the time.

$$\frac{\partial}{\partial t}\left[\int_{\mathcal{L}(\tau)}\boldsymbol{W}\;\boldsymbol{dl_\tau}\right]=\oint_{\mathcal{L}(\tau)}\boldsymbol{\alpha}\times\boldsymbol{v}^{\boldsymbol{d}}\;\boldsymbol{dl_\tau} \tag{75}$$

This can now be pulled back, to the configuration at time τ, using $\boldsymbol{F_\tau}$: (As if, in the new parametrization, time t is the initial configuration).

$$\frac{\partial}{\partial t}\left[\int_{\mathcal{L}(t)}\boldsymbol{W}\;\boldsymbol{F_\tau}\;\boldsymbol{dL_t}\right]=\oint_{\mathcal{L}(t)}\boldsymbol{\alpha}\times\boldsymbol{v}^{\boldsymbol{d}}\,\boldsymbol{F_\tau}\;\boldsymbol{dL_t}\quad\Rightarrow\quad\int_{\mathcal{L}(t)}\dot{\overline{\boldsymbol{W}\,\boldsymbol{F_\tau}}}\;\boldsymbol{dL_t}=\oint_{\mathcal{L}(t)}\boldsymbol{\alpha}\times\boldsymbol{v}^{\boldsymbol{d}}\,\boldsymbol{F_\tau}\;\boldsymbol{dl_t} \tag{76}$$

Since localization theorem doesn't hold along arbitrary curves, we use Stokes theorem to switch into surface integration:

$$\int_{\mathcal{A}(t)}\mathbf{curl}\left(\dot{\overline{\boldsymbol{W}\,\boldsymbol{F_\tau}}}-\boldsymbol{\alpha}\times\boldsymbol{v}^{\boldsymbol{d}}\,\boldsymbol{F_\tau}\right)\boldsymbol{da_t}=0 \tag{77}$$

Using the localization theorem, and ignorning any additive gradient of some vector field ($\mathbf{curl}\,\nabla\boldsymbol{f}=0\;\forall\boldsymbol{f}$), one writes :

$$\dot{\overline{\boldsymbol{W}\,\boldsymbol{F_\tau}}}=\boldsymbol{\alpha}\times\boldsymbol{v}^{\boldsymbol{d}}\,\boldsymbol{F_\tau} \tag{78}$$

Ignorning the additional $\nabla\boldsymbol{f}$, is justified by the fact thet localization is a microscopic statement and at a microscopic level, plastic deformation can only occur due to dislocation motion: the term $\boldsymbol{\alpha}\times\boldsymbol{v}^{\boldsymbol{d}}$ is responsible for that. Arranging the terms gives : ($\dot{(\,)}$ is the material derivative)

$$\dot{\boldsymbol{W}}\,\boldsymbol{F_\tau}+\boldsymbol{W}\,\boldsymbol{L_\tau}\,\boldsymbol{F_\tau}=(\boldsymbol{\alpha}\times\boldsymbol{v}^{\boldsymbol{d}})\boldsymbol{F_\tau} \tag{79}$$

Evaluating at $\tau=0$ yields the desired result: ($\boldsymbol{F_\tau}=\boldsymbol{1}$)

$$\boxed{\dot{\boldsymbol{W}}+\boldsymbol{W}\,\boldsymbol{L}=\boldsymbol{\alpha}\times\boldsymbol{v}^{\boldsymbol{d}}} \tag{80}$$

This statement, it appears to me in spirit, as a large deformation generlization of Kosevich's observation that time derivative of elastic distortion and the spatial gradient of the velocity field do not balance with each other when dislocation are moving.
In his work, Acharya 2015, shows an intersting result by an easy algebraic manupulation of 80. In fact, $\boldsymbol{W} = \boldsymbol{F_e}^{-1}$, and we can isolate $\boldsymbol{L}$ from the previous equation:

$$\boldsymbol{L} = -\boldsymbol{F_e}\dot{\boldsymbol{F_e}^{-1}} + (\boldsymbol{F_e}\boldsymbol{\alpha}) \times \boldsymbol{v^d} \tag{81}$$

But, as seen previously

$$\boldsymbol{F_e}\,\boldsymbol{F_e}^{-1} = \boldsymbol{I}_3 = \quad \Rightarrow \quad \dot{\boldsymbol{F}}_e\,\boldsymbol{F_e}^{-1} + \boldsymbol{F_e}\,\dot{\boldsymbol{F_e}^{-1}} = 0 \quad \Rightarrow \quad \dot{\boldsymbol{F}}_e\,\boldsymbol{F_e}^{-1} = -\boldsymbol{F_e}\,\dot{\boldsymbol{F_e}^{-1}} \tag{82}$$

Finally,

$$\boxed{\boldsymbol{L} = \underbrace{\dot{\boldsymbol{F}}_e\,\boldsymbol{F_e}^{-1}}_{\boldsymbol{L_e}} + \underbrace{(\boldsymbol{F_e}\boldsymbol{\alpha}) \times \boldsymbol{v^d}}_{\boldsymbol{L_p}}} \tag{83}$$

This may be interpreted as a fundamental additive decomposition of the velocity gradient into elastic part $\boldsymbol{L_e}$ and plastic part $\boldsymbol{L_p}$. The latter is defined by the rate of deformation produced by the flow of dislo- cation lines in the current configuration, without any reference to the notion of a pre-assigned reference configuration or a total plastic deformation from it. We bypassed any need of multiplicative decomposition of the gradient of deformation.

8 Constitutive analysis

Following Colleman-Noll procedure XXX

8.1 Mass balance

8.2 Momentum balance

8.3 Energy Balance

8.4 Entropy imbalance

Starting from the 2^{nd} principle of thermodynamics, the entropy density η must satisfy :

$$\frac{d}{dt}\left[\int_\Omega \rho\eta\, dv\right] \geq 0 \tag{84}$$

Using Legendre transformation we introduce Helmholtz free energy density $\psi := \varepsilon - \eta\theta$. In an isothermal case, the previous inequality is simply equivalent to:

$$\mathcal{D} = \int_\Omega \rho\dot{\varepsilon}\, dv - \int_\Omega \dot{\psi}\, dv \geq 0 \tag{85}$$

Were $\mathcal{D}$ is the dissipation. Using energy balance, we have $\rho\dot{\varepsilon} = \boldsymbol{\sigma} : \boldsymbol{L}$. So that, the dissipation becomes:

$$\mathcal{D} = \int_\Omega \boldsymbol{\sigma} : \boldsymbol{L}\, dv - \int_\Omega \dot{\psi}\, dv \geq 0 \tag{86}$$

We suppose, in the most general case, that the free energy density ψ is a function of elastic distortion $\boldsymbol{W}$ and the dislocation density α:

$$\psi := \psi(\boldsymbol{W}, \boldsymbol{\alpha}) \quad \Rightarrow \quad \dot{\psi} = \frac{\partial\psi}{\partial\,\boldsymbol{W}} : \dot{\boldsymbol{W}} + \frac{\partial\psi}{\partial\boldsymbol{\alpha}} : \dot{\boldsymbol{\alpha}} \tag{87}$$

Using the evolution laws 69 and 80, we get :

$$\dot{\psi} = \frac{\partial\psi}{\partial\,\boldsymbol{W}} : \left(-\boldsymbol{W}\,\boldsymbol{L} + \boldsymbol{\alpha} \times \boldsymbol{v^d}\right) + \frac{\partial\psi}{\partial\boldsymbol{\alpha}} : \left[-(\mathbf{Tr}\,\boldsymbol{L})\,\boldsymbol{\alpha} + +\boldsymbol{\alpha}\,\boldsymbol{L}^t - \mathbf{curl}\,\boldsymbol{\alpha} \times \boldsymbol{v^d}\right] \tag{88}$$

Let's now manipulate each term to show conjugate variables. We note that:

$$\frac{\partial \psi}{\partial \boldsymbol{W}} : \boldsymbol{W}\boldsymbol{L} = \boldsymbol{W}^t \frac{\partial \psi}{\partial \boldsymbol{W}} : \boldsymbol{L} \quad \text{and} \quad \frac{\partial \psi}{\partial \boldsymbol{\alpha}} : \boldsymbol{\alpha}\boldsymbol{L}^t = \boldsymbol{\alpha}^t \frac{\partial \psi}{\partial \boldsymbol{\alpha}} : \boldsymbol{L}^t = \left(\frac{\partial \psi}{\partial \boldsymbol{\alpha}}\right)^t \boldsymbol{\alpha} : \boldsymbol{L} \tag{89}$$

And that:

$$\frac{\partial \psi}{\partial \boldsymbol{W}} : (\boldsymbol{\alpha} \times \boldsymbol{v^d}) = \partial_{\boldsymbol{W}} \psi_{ij} \mathcal{E}_{jkl} \alpha_{ik} v_l^d = \partial_{\boldsymbol{W}} \psi_{ij} \alpha_{ik} \mathcal{E}_{jkl} v_l^d = \left[\left(\frac{\partial \psi}{\partial \boldsymbol{W}}\right)^t \boldsymbol{\alpha} : \boldsymbol{\mathcal{E}}\right] \cdot \boldsymbol{v^d} \tag{90}$$

In addition to :

$$\frac{\partial \psi}{\partial \boldsymbol{\alpha}} : (\mathbf{Tr}\, \boldsymbol{L})\boldsymbol{\alpha} = (\mathbf{Tr}\, \boldsymbol{L}) \left(\frac{\partial \psi}{\partial \boldsymbol{\alpha}} : \boldsymbol{\alpha}\right) = (\boldsymbol{1} : \boldsymbol{L}) \left(\frac{\partial \psi}{\partial \boldsymbol{\alpha}} : \boldsymbol{\alpha}\right) = \left[\left(\frac{\partial \psi}{\partial \boldsymbol{\alpha}} : \boldsymbol{\alpha}\right) \boldsymbol{1}\right] : \boldsymbol{L} \tag{91}$$

Replacing in the definition of $\mathcal{D}$, we get:

$$\mathcal{D} = \int_\Omega \left[\boldsymbol{\sigma} + \rho \boldsymbol{W}^t \frac{\partial \psi}{\partial \boldsymbol{W}} - \rho \left(\frac{\partial \psi}{\partial \boldsymbol{\alpha}}\right)^t \boldsymbol{\alpha} - \rho \left(\frac{\partial \psi}{\partial \boldsymbol{\alpha}} : \boldsymbol{\alpha}\right) \boldsymbol{1}\right] : \boldsymbol{L}\, dv - \int_\Omega \left[\rho \left(\frac{\partial \psi}{\partial \boldsymbol{W}}\right)^t \boldsymbol{\alpha} : \boldsymbol{\mathcal{E}}\right] \cdot \boldsymbol{v^d}\, dv$$
$$+ \int_\Omega \frac{\partial \psi}{\partial \boldsymbol{\alpha}} : \mathbf{curl}\, \boldsymbol{\alpha} \times \boldsymbol{v^d}\, dv$$

The last term is also re-arranged using the following tensor identity:

$$\int_\Omega \boldsymbol{A} : \mathbf{curl}\, \boldsymbol{B} = \int_\Omega \mathbf{curl}\, \boldsymbol{A} : \boldsymbol{B}\, dv - \int_{\partial\Omega} \boldsymbol{A} : (\boldsymbol{B} \times \boldsymbol{n})\, da \tag{92}$$

So,

$$\int_\Omega \rho \frac{\partial \psi}{\partial \boldsymbol{\alpha}} : \mathbf{curl}\, \boldsymbol{\alpha} \times \boldsymbol{v^d} = \int_\Omega \mathbf{curl} \left(\rho \frac{\partial \psi}{\partial \boldsymbol{\alpha}}\right) : \boldsymbol{\alpha} \times \boldsymbol{v^d}\, dv - \int_{\partial\Omega} \rho \frac{\partial \psi}{\partial \boldsymbol{\alpha}} : \left[(\boldsymbol{\alpha} \times \boldsymbol{v^d}) \times \boldsymbol{n}\right]\, da$$
$$\int_\Omega \left[\left(\mathbf{curl} \left(\rho \frac{\partial \psi}{\partial \boldsymbol{\alpha}}\right)\right)^t \boldsymbol{\alpha} : \boldsymbol{\mathcal{E}}\right] \cdot \boldsymbol{v^d}\, dv - \int_{\partial\Omega} \rho \frac{\partial \psi}{\partial \boldsymbol{\alpha}} : \left[(\boldsymbol{\alpha} \times \boldsymbol{v^d}) \times \boldsymbol{n}\right]\, da$$

Finally, we assemble everything :

$$\mathcal{D} = \int_\Omega \left[\boldsymbol{\sigma} + \rho \boldsymbol{W}^t \frac{\partial \psi}{\partial \boldsymbol{W}} - \rho \left(\frac{\partial \psi}{\partial \boldsymbol{\alpha}}\right)^t \boldsymbol{\alpha} - \rho \left(\frac{\partial \psi}{\partial \boldsymbol{\alpha}} : \boldsymbol{\alpha}\right) \boldsymbol{1}\right] : \boldsymbol{L}\, dv - \int_\Omega \underbrace{\left\{\left[\rho \left(\frac{\partial \psi}{\partial \boldsymbol{W}}\right) - \mathbf{curl} \left(\rho \frac{\partial \psi}{\partial \boldsymbol{\alpha}}\right)\right]^t \boldsymbol{\alpha} : \boldsymbol{\mathcal{E}}\right\}}_{\text{Driving force } f^d} \cdot \boldsymbol{v^d}\, dv$$
$$- \int_{\partial\Omega} \rho \frac{\partial \psi}{\partial \boldsymbol{\alpha}} : \left[(\boldsymbol{\alpha} \times \boldsymbol{v^d}) \times \boldsymbol{n}\right]\, da \geq 0$$

The previous re-arragement exposes the driving force acting on the dislocations (as conjugate to their velocity $\boldsymbol{v^d}$). The driving force $\boldsymbol{f^d}$ is :

$$\boxed{\boldsymbol{f^d} := \left[\rho \left(\frac{\partial \psi}{\partial \boldsymbol{W}}\right) - \mathbf{curl} \left(\rho \frac{\partial \psi}{\partial \boldsymbol{\alpha}}\right)\right]^t \boldsymbol{\alpha} : \boldsymbol{\mathcal{E}}} \tag{93}$$

This dissipative inequality give insights as well as constraints on the constitutive prescription of the stress-elastic distortion relationship and on the velocity of dislocations. In the absence of any dislocation, do disspation occurs, and ....

Bibliography

Acharya, A. (2001). A model of crystal plasticity based on the theory of continuously distributed dislocations. *Journal of the Mechanics and Physics of Solids*, *49*(4), 761–784. https://doi.org/10.1016/S0022-5096(00)00060-0

Acharya, A. (2003). Driving forces and boundary conditions in continuum dislocation mechanics. *Proceedings of the Royal Society of London. Series A: Mathematical, Physical and Engineering Sciences*, *459*(2034), 1343–1363. https://doi.org/10.1098/rspa.2002.1095

Acharya, A. (2004). Constitutive analysis of finite deformation field dislocation mechanics. *Journal of the Mechanics and Physics of Solids*, *52*(2), 301–316. https://doi.org/10.1016/S0022-5096(03)00093-0

Acharya, A. (2010). New inroads in an old subject: Plasticity, from around the atomic to the macroscopic scale. *Journal of the Mechanics and Physics of Solids*, *58*(5), 766–778. https://doi.org/10.1016/j.jmps.2010.02.001

Acharya, A. (2011). Microcanonical Entropy and Mesoscale Dislocation Mechanics and Plasticity. *Journal of Elasticity*, *104*(1-2), 23–44. https://doi.org/10.1007/s10659-011-9328-3

Acharya, A. (2018, September). Stress of a spatially uniform dislocation density field.

Acharya, A., Angheluta, L., & Viñals, J. (2022). Elasticity versus phase field driven motion in the phase field crystal model. *Modelling and Simulation in Materials Science and Engineering*, *30*(6), 064005. https://doi.org/10.1088/1361-651X/ac860b

Acharya, A., & Roy, A. (2006). Size effects and idealized dislocation microstructure at small scales: Predictions of a Phenomenological model of Mesoscopic Field Dislocation Mechanics: Part I. *Journal of the Mechanics and Physics of Solids*, *54*(8), 1687–1710. https://doi.org/10.1016/j.jmps.2006.01.009

Acharya, A., & Tartar, L. (2011). On an equation from the theory of field dislocation mechanics.

Acharya, A., & Viñals, J. (2020). Field dislocation mechanics and phase field crystal models. *Physical Review B*, *102*(6), 064109. https://doi.org/10.1103/PhysRevB.102.064109

Acharya, A., & Zhang, X. (2015). From dislocation motion to an additive velocity gradient decomposition, and some simple models of dislocation dynamics. *Chinese Annals of Mathematics, Series B*, *36*(5), 645–658. https://doi.org/10.1007/s11401-015-0970-0

Angheluta, L., Jeraldo, P., & Goldenfeld, N. (2012). Anisotropic velocity statistics of topological defects under shear flow. *Physical Review E*, *85*(1), 011153. https://doi.org/10.1103/PhysRevE.85.011153

Archer, A. J., Ratliff, D. J., Rucklidge, A. M., & Subramanian, P. (2019). Deriving phase field crystal theory from dynamical density functional theory: Consequences of the approximations. *Physical Review E*, *100*(2), 022140. https://doi.org/10.1103/PhysRevE.100.022140

Arora, R. (2019, March). *Computational Approximation of Mesoscale Field Dislocation Mechanics at Finite Deformation* [Thesis]. Carnegie Mellon University. https://doi.org/10.1184/R1/7797896.v1

Arora, R., & Acharya, A. (2020). Dislocation pattern formation in finite deformation crystal plasticity. *International Journal of Solids and Structures*, *184*, 114–135. https://doi.org/10.1016/j.ijsolstr.2019.02.013

Arora, R., Zhang, X., & Acharya, A. (2020). Finite element approximation of finite deformation dislocation mechanics. *Computer Methods in Applied Mechanics and Engineering*, *367*, 113076. https://doi.org/10.1016/j.cma.2020.113076

Athreya, B. P., Goldenfeld, N., & Dantzig, J. A. (2006). Renormalization-group theory for the phase-field crystal equation. *Physical Review E*, *74*(1), 011601. https://doi.org/10.1103/PhysRevE.74.011601

Bénard, H. (1901). Les tourbillons cellulaires dans une nappe liquide. - Méthodes optiques d'observation et d'enregistrement. *Journal de Physique Théorique et Appliquée*, *10*(1), 254–266. https://doi.org/10.1051/jphystap:0190100100025400

Berdichevsky, V. L. (2006). Continuum theory of dislocations revisited. *Continuum Mechanics and Thermodynamics*, *18*(3-4), 195–222. https://doi.org/10.1007/s00161-006-0024-7

Berry, J., Grant, M., & Elder, K. R. (2006). Diffusive atomistic dynamics of edge dislocations in two dimensions. *Physical Review E*, *73*(3), 031609. https://doi.org/10.1103/PhysRevE.73.031609

Bertin, N., Aubry, S., Arsenlis, A., & Cai, W. (2019). GPU-accelerated dislocation dynamics using subcycling time-integration. *Modelling and Simulation in Materials Science and Engineering*, *27*(7), 075014. https://doi.org/10.1088/1361-651X/ab3a03

Bilby, B. A., Bullough, R., Smith, E., & Whittaker, J. M. (1955). Continuous distributions of dislocations: A new application of the methods of non-Riemannian geometry. *Proceedings of the Royal Society of London. Series A. Mathematical and Physical Sciences*, *231*(1185), 263–273. https://doi.org/10.1098/rspa.1955.0171

Bulatov, V., & Cai, W. (2006, November). *Computer Simulations of Dislocations*. OUP Oxford.

Chan, P. Y., Tsekenis, G., Dantzig, J., Dahmen, K. A., & Goldenfeld, N. (2010). Plasticity and Dislocation Dynamics in a Phase Field Crystal Model. *Physical Review Letters*, *105*(1), 015502. https://doi.org/10.1103/PhysRevLett.105.015502

Cui, Y., Li, K., Wang, C., & Liu, W. (2021). Dislocation evolution during additive manufacturing of tungsten. *Modelling and Simulation in Materials Science and Engineering*, *30*(2), 024001. https://doi.org/10.1088/1361-651X/ac40d3

Devincre, B., Pontikis, V., Brechet, Y., Canova, G., Condat, M., & Kubin, L. (1992). Three-Dimensional Simulations of Plastic Flow in Crystals. In M. Mareschal & B. L. Holian (Eds.), *Microscopic Simulations of Complex Hydrodynamic Phenomena* (pp. 413–423). Springer US. https://doi.org/10.1007/978-1-4899-2314-1_28

Elder, K. R., & Grant, M. (2004). Modeling elastic and plastic deformations in nonequilibrium processing using phase field crystals. *Physical Review E*, *70*(5), 051605. https://doi.org/10.1103/PhysRevE.70.051605

Elder, K. R., Katakowski, M., Haataja, M., & Grant, M. (2002). Modeling Elasticity in Crystal Growth. *Physical Review Letters*, *88*(24), 245701. https://doi.org/10.1103/PhysRevLett.88.245701

Elder, K. R., Provatas, N., Berry, J., Stefanovic, P., & Grant, M. (2007a). Phase-field crystal modeling and classical density functional theory of freezing. *Physical Review B*, *75*(6), 064107. https://doi.org/10.1103/PhysRevB.75.064107

Elder, K. R., Provatas, N., Berry, J., Stefanovic, P., & Grant, M. (2007b). Phase-field crystal modeling and classical density functional theory of freezing. *Physical Review B*, *75*(6), 064107. https://doi.org/10.1103/PhysRevB.75.064107

Engel, E., & Dreizler, R. M. (2011). *Density Functional Theory: An Advanced Course*. Springer Berlin Heidelberg. https://doi.org/10.1007/978-3-642-14090-7

Fox, N. (1966). A Continuum Theory of Dislocations for Single Crystals. *IMA Journal of Applied Mathematics*, *2*(4), 285–298. https://doi.org/10.1093/imamat/2.4.285

Frenkel, J. (1926). Zur Theorie der Elastizitätsgrenze und der Festigkeit kristallinischer Körper. *Zeitschrift für Physik*, *37*(7), 572–609. https://doi.org/10.1007/BF01397292

Fressengeas, C. (2017). *Mechanics of dislocation fields*. ISTE, Ltd.

Greenwood, M., Rottler, J., & Provatas, N. (2011). Phase-field-crystal methodology for modeling of structural transformations. *Physical Review E*, *83*(3), 031601. https://doi.org/10.1103/PhysRevE.83.031601

Halperin, B. (1981). Physics of defects. In *Physics of Defects* (R. Balian, M. Kleman, and J.-P. Poirier, pp. 814–857).

Heinonen, V., Achim, C. V., Kosterlitz, J. M., Ying, S.-C., Lowengrub, J., & Ala-Nissila, T. (2016). Consistent Hydrodynamics for Phase Field Crystals. *Physical Review Letters*, *116*(2), 024303. https://doi.org/10.1103/PhysRevLett.116.024303

Hochrainer, T., Zaiser, M., & Gumbsch, P. (2007). A three-dimensional continuum theory of dislocation systems: Kinematics and mean-field formulation. *Philosophical Magazine*, *87*(8-9), 1261–1282. https://doi.org/10.1080/14786430600930218

Hochrainer, T., Sandfeld, S., Zaiser, M., & Gumbsch, P. (2014). Continuum dislocation dynamics: Towards a physical theory of crystal plasticity. *Journal of the Mechanics and Physics of Solids*, *63*, 167–178. https://doi.org/10.1016/j.jmps.2013.09.012

Jaatinen, A., & Ala-Nissila, T. (2010). Extended phase diagram of the three-dimensional phase field crystal model. *Journal of Physics: Condensed Matter*, *22*(20), 205402. https://doi.org/10.1088/0953-8984/22/20/205402

Kochmann, D. M. (2009, September). *Mechanical modeling of microstructures in elasto-plastically deformed crystalline solids* [Doctoral dissertation].

Kosevich, A. M. (1965). DYNAMICAL THEORY OF DISLOCATIONS.

Kröner, E. (2001). Benefits and shortcomings of the continuous theory of dislocations. *International Journal of Solids and Structures*, *38*(6), 1115–1134. https://doi.org/10.1016/S0020-7683(00)00077-9

Kröner, E. (1959). Allgemeine Kontinuumstheorie der Versetzungen und Eigenspannungen. *Archive for Rational Mechanics and Analysis*, *4*(1), 273–334. https://doi.org/10.1007/BF00281393

Kubin, L. P., & Canova, G. (1992). The modelling of dislocation patterns. *Scripta Metallurgica et Materialia*, *27*(8), 957–962. https://doi.org/10.1016/0956-716X(92)90456-O

Lima-Chaves, G. D., & Upadhyay, M. V. (2024). Finite element implementation of the thermal field dislocation mechanics model: Study of temperature evolution due to dislocation activity. *Computer Methods in Applied Mechanics and Engineering*, *421*, 116763. https://doi.org/10.1016/j.cma.2024.116763

Majaniemi, S., & Grant, M. (2007). Dissipative phenomena and acoustic phonons in isothermal crystals: A density-functional theory study. *Physical Review B*, *75*(5), 054301. https://doi.org/10.1103/PhysRevB.75.054301

Majaniemi, S., Nonomura, M., & Grant, M. (2008). First-principles and phenomenological theories of hydrodynamics of solids. *The European Physical Journal B*, *66*(3), 329–335. https://doi.org/10.1140/epjb/e2008-00436-x

Mazenko, G. F. (1997). Vortex Velocities in the $\mathit{O}(\mathit{n})$ Symmetric Time-Dependent Ginzburg-Landau Model. *Physical Review Letters*, *78*(3), 401–404. https://doi.org/10.1103/PhysRevLett.78.401

Mazenko, G. F. (1999). Velocity distribution for strings in phase-ordering kinetics. *Physical Review E*, *59*(2), 1574–1584. https://doi.org/10.1103/PhysRevE.59.1574

Mazenko, G. F., & Wickham, R. A. (1998). Ordering kinetics of defect structures. *Physical Review E*, *57*(3), 2539–2542. https://doi.org/10.1103/PhysRevE.57.2539

Mermin, N. D. (1979). The topological theory of defects in ordered media. *Reviews of Modern Physics*, *51*(3), 591–648. https://doi.org/10.1103/RevModPhys.51.591

Mkhonta, S. K., Elder, K. R., & Huang, Z.-F. (2013). Exploring the Complex World of Two-Dimensional Ordering with Three Modes. *Physical Review Letters*, *111*(3), 035501. https://doi.org/10.1103/PhysRevLett.111.035501

Mügge, O. (1883). Neues Jahrbuch für Mineralogie 13.

Mura, T. (1963). Continuous distribution of moving dislocations. *Philosophical Magazine*, *8*(89), 843–857. https://doi.org/10.1080/14786436308213841

Nabarro, F. R. N. (1947). Dislocations in a simple cubic lattice. *Proceedings of the Physical Society*, *59*(2), 256–272. https://doi.org/10.1088/0959-5309/59/2/309

Nelson, D. R., & Toner, J. (1981). Bond-orientational order, dislocation loops, and melting of solids and smectic-A liquid crystals. *Physical Review B*, *24*(1), 363–387. https://doi.org/10.1103/PhysRevB.24.363

Nye, J. (1953). Some Geometrical Relations In Dislocated Crystaals. *Acta Metallurgica*, *1*, 153–162. https://doi.org/10.1016/0001-6160(53)90054-6

Olmsted, D. L., Jr, L. G. H., Curtin, W. A., & Clifton, R. J. (2004, December). Atomistic simulations of dislocation mobility in Al, Ni and Al/Mg alloys. https://doi.org/10.48550/arXiv.cond-mat/0412324

Orowan, E. (n.d.). *Zeitschrift für Physik*, *89*, 605–613, 614–633, 634–659.
Payne, M. C., Robertson, I. J., Thomson, D., & Heine, V. (1996). Ab initio databases for fitting and testing interatomic potentials. *Philosophical Magazine B*, *73*(1), 191–199. https://doi.org/10.1080/13642819608239124
Peierls, R. (1940). The size of a dislocation. *Proceedings of the Physical Society*, *52*(1), 34. https://doi.org/10.1088/0959-5309/52/1/305
Pismen, L. M. (1999). Vortices in Nonlinear Fields: From Liquid Crystals to Superfluids, from Non-Equilibrium Patterns to Cosmic Strings.
Podmaniczky, F., & Gránásy, L. (2021). Nucleation and Post-Nucleation Growth in Diffusion-Controlled and Hydrodynamic Theory of Solidification. *Crystals*, *11*(4), 437. https://doi.org/10.3390/cryst11040437
Polanyi, M. (n.d.). *Zeitschrift für Physik*, *89*, 660.
Proville, L., Rodney, D., & Marinica, M.-C. (2012). Quantum effect on thermally activated glide of dislocations. *Nature Materials*, *11*(10), 845–849. https://doi.org/10.1038/nmat3401
Rao, S. I., Dimiduk, D. M., Parthasarathy, T. A., El-Awady, J., Woodward, C., & Uchic, M. D. (2011). Calculations of intersection cross-slip activation energies in fcc metals using nudged elastic band method. *Acta Materialia*, *59*(19), 7135–7144. https://doi.org/10.1016/j.actamat.2011.08.029
Rayleigh, L. (1916). LIX. *On convection currents in a horizontal layer of fluid, when the higher temperature is on the under side*. *The London, Edinburgh, and Dublin Philosophical Magazine and Journal of Science*, *32*(192), 529–546. https://doi.org/10.1080/14786441608635602
Rodney, D., Ventelon, L., Clouet, E., Pizzagalli, L., & Willaime, F. (2017). Ab initio modeling of dislocation core properties in metals and semiconductors. *Acta Materialia*, *124*, 633–659. https://doi.org/10.1016/j.actamat.2016.09.049
Roy, A. (2005). Finite element approximation of field dislocation mechanics. *Journal of the Mechanics and Physics of Solids*, *53*(1), 143–170. https://doi.org/10.1016/j.jmps.2004.05.007
Salvalaglio, M., Angheluta, L., Huang, Z.-F., Voigt, A., Elder, K. R., & Viñals, J. (2020). A coarse-grained phase-field crystal model of plastic motion. *Journal of the Mechanics and Physics of Solids*, *137*, 103856. https://doi.org/10.1016/j.jmps.2019.103856
Sandfeld, S., Hochrainer, T., Zaiser, M., & Gumbsch, P. (2011). Continuum modeling of dislocation plasticity: Theory, numerical implementation, and validation by discrete dislocation simulations. *Journal of Materials Research*, *26*(5), 623–632. https://doi.org/10.1557/jmr.2010.92
Shiwa, Y., & Kawasaki, K. (1986). Dislocation motion and vertical vorticity in Rayleigh-Benard convective structures. *Journal of Physics A: Mathematical and General*, *19*(8), 1387. https://doi.org/10.1088/0305-4470/19/8/020
Siggia, E. D., & Zippelius, A. (1981). Dynamics of defects in Rayleigh-Bénard convection. *Physical Review A*, *24*(2), 1036–1049. https://doi.org/10.1103/PhysRevA.24.1036
Skaugen, A., Angheluta, L., & Viñals, J. (2018a). Dislocation dynamics and crystal plasticity in the phase-field crystal model. *Physical Review B*, *97*(5), 054113. https://doi.org/10.1103/PhysRevB.97.054113
Skaugen, A., Angheluta, L., & Viñals, J. (2018b). Separation of Elastic and Plastic Timescales in a Phase Field Crystal Model. *Physical Review Letters*, *121*(25), 255501. https://doi.org/10.1103/PhysRevLett.121.255501
Skogvoll, V., Angheluta, L., Skaugen, A., Salvalaglio, M., & Viñals, J. (2022). A phase field crystal theory of the kinematics of dislocation lines. *Journal of the Mechanics and Physics of Solids*, *166*, 104932. https://doi.org/10.1016/j.jmps.2022.104932
Skogvoll, V., Rønning, J., Salvalaglio, M., & Angheluta, L. (2023). A unified field theory of topological defects and non-linear local excitations. *npj Computational Materials*, *9*(1), 1–13. https://doi.org/10.1038/s41524-023-01077-6

Skogvoll, V., Salvalaglio, M., & Angheluta, L. (2022, September). Hydrodynamic phase field crystal approach to interfaces, dislocations, and multi-grain networks. https://doi.org/10.48550/arXiv.2205.12788

Skogvoll, V., Skaugen, A., Angheluta, L., & Viñals, J. (2021). Dislocation nucleation in the phase-field crystal model. *Physical Review B*, *103*(1), 014107. https://doi.org/10.1103/PhysRevB.103.014107

Spearot, D. E., & Sangid, M. D. (2014). Insights on slip transmission at grain boundaries from atomistic simulations. *Current Opinion in Solid State and Materials Science*, *18*(4), 188–195. https://doi.org/10.1016/j.cossms.2014.04.001

Stefanovic, P., Haataja, M., & Provatas, N. (2006). Phase-Field Crystals with Elastic Interactions. *Physical Review Letters*, *96*(22), 225504. https://doi.org/10.1103/PhysRevLett.96.225504

Stefanovic, P., Haataja, M., & Provatas, N. (2009). Phase field crystal study of deformation and plasticity in nanocrystalline materials. *Physical Review E*, *80*(4), 046107. https://doi.org/10.1103/PhysRevE.80.046107

Stukowski, A., & Albe, K. (2010). Extracting dislocations and non-dislocation crystal defects from atomistic simulation data. *Modelling and Simulation in Materials Science and Engineering*, *18*(8), 085001. https://doi.org/10.1088/0965-0393/18/8/085001

Swift, J., & Hohenberg, P. C. (1977). Hydrodynamic fluctuations at the convective instability. *Physical Review A*, *15*(1), 319–328. https://doi.org/10.1103/PhysRevA.15.319

T. Arsenlis, V. Bulatov, W. Cai, G. Hommes, M. Rhee, and M. Tang. (2021). ParaDis.

Taylor, G. I. (1934). The Mechanism of Plastic Deformation of Crystals. Part I. Theoretical. *Proceedings of the Royal Society of London. Series A, Containing Papers of a Mathematical and Physical Character*, *145*(855), 362–387.

Thompson, A. P., Aktulga, H. M., Berger, R., Bolintineanu, D. S., Brown, W. M., Crozier, P. S., in 't Veld, P. J., Kohlmeyer, A., Moore, S. G., Nguyen, T. D., Shan, R., Stevens, M. J., Tranchida, J., Trott, C., & Plimpton, S. J. (2022). LAMMPS - a flexible simulation tool for particle-based materials modeling at the atomic, meso, and continuum scales. *Computer Physics Communications*, *271*, 108171. https://doi.org/10.1016/j.cpc.2021.108171

Toner, J., & Nelson, D. R. (1981). Smectic, cholesteric, and Rayleigh-Benard order in two dimensions. *Physical Review B*, *23*(1), 316–334. https://doi.org/10.1103/PhysRevB.23.316

Tóth, G. I., Gránásy, L., & Tegze, G. (2013). Nonlinear hydrodynamic theory of crystallization. *Journal of Physics: Condensed Matter*, *26*(5), 055001. https://doi.org/10.1088/0953-8984/26/5/055001

TriDis. (2021).

Upadhyay, M. V. (2020). On the thermo-mechanical theory of field dislocations in transient heterogeneous temperature fields. *Journal of the Mechanics and Physics of Solids*, *145*, 104150. https://doi.org/10.1016/j.jmps.2020.104150

Upadhyay, M. V., & Viñals, J. (2024). Coupling Phase Field Crystal and Field Dislocation Mechanics for a consistent description of dislocation structure and elasticity. *European Journal of Mechanics - A/Solids*, *108*, 105419. https://doi.org/10.1016/j.euromechsol.2024.105419

Varadhan, S. N., Beaudoin, A. J., Acharya, A., & Fressengeas, C. (2006). Dislocation transport using an explicit Galerkin/least-squares formulation. *Modelling and Simulation in Materials Science and Engineering*, *14*(7), 1245–1270. https://doi.org/10.1088/0965-0393/14/7/011

Voltera. (1907). Sur l'equilibre des cirps elastiques multiplement connexes. *Ann. Ecole Norm. Super*, *24*, 401–517.

Willis, J. R. (1967a). Second-order effects of dislocations in anisotropic crystals. *International Journal of Engineering Science*, *5*(2), 171–190. https://doi.org/10.1016/0020-7225(67)90003-1

Willis, J. R. (1967b). Second-order effects of dislocations in anisotropic crystals. *International Journal of Engineering Science*, *5*(2), 171–190. https://doi.org/10.1016/0020-7225(67)90003-1

Woodward, C., Trinkle, D. R., Hector, L. G., & Olmsted, D. L. (2008). Prediction of Dislocation Cores in Aluminum from Density Functional Theory. *Physical Review Letters*, *100*(4), 045507. https://doi.org/10.1103/PhysRevLett.100.045507

Wu, K.-A., & Karma, A. (2007). Phase-field crystal modeling of equilibrium bcc-liquid interfaces. *Physical Review B*, *76*(18), 184107. https://doi.org/10.1103/PhysRevB.76.184107

Zhang, X., Acharya, A., Walkington, N. J., & Bielak, J. (2015). A single theory for some quasi-static, supersonic, atomic, and tectonic scale applications of dislocations. *Journal of the Mechanics and Physics of Solids*, *84*, 145–195. https://doi.org/10.1016/j.jmps.2015.07.004

Zhou, S. J., Preston, D. L., Lomdahl, P. S., & Beazley, D. M. (1998). Large-scale molecular dynamics simulations of dislocation intersection in copper. *Science* (*New York, N.Y.*), *279*(5356), 1525–1527. https://doi.org/10.1126/science.279.5356.1525

Zhou, W., Wang, J., Wang, Z., & Huang, Z.-F. (2019). Mechanical relaxation and fracture of phase field crystals. *Physical Review E*, *99*(1), 013302. https://doi.org/10.1103/PhysRevE.99.013302

Zhou, X. W., Sills, R. B., Ward, D. K., & Karnesky, R. A. (2017). Atomistic calculations of dislocation core energy in aluminium. *Physical Review B*, *95*(5), 054112. https://doi.org/10.1103/PhysRevB.95.054112